X-RAY EMISSION FROM COMPACT SOURCES

Lynn Cominsky*
Department of Physics and Astronomy
Sonoma State University, Rohnert Park, CA 94928

and

Stanford Linear Accelerator Center
Stanford University, Stanford, CA 94309

ABSTRACT

This paper presents a review of the physical parameters of neutron stars and black holes that have been derived from X-ray observations. I then explain how these physical parameters can be used to learn about the extreme conditions occurring in regions of strong gravity, and present some recent evidence for relativistic effects seen in these systems. A glossary of commonly used terms and a short tutorial on the names of X-ray sources are also included.

*Supported by NSF grant PHYS-9722126 and DOE Contract DE-AC03-76SF00515.1

1 Overview

X-ray emission from compact objects was discovered in 1962,[1] with the detection of what we now know as a neutron star in the low mass binary, Sco X-1. In the past 35 years, the field has matured, and satellite based X-ray observations of neutron star and black hole binaries are conducted by scientists from many different nations, and with many different instruments. Recently, the increased collecting area and high time resolution of satellites such as NASA's Rossi X-ray Timing Explorer have produced data that have broken new ground in allowing high-energy astrophysicists to make physical measurements of compact binaries. Unobtainable in earth-bound laboratories, X-ray satellite observations remain the best way to study the effects of strong field gravity and to test the predictions of General Relativity in this regime.

In this paper, I will review the basic physics which produces X-ray emission from neutron stars and black holes, focusing primarily on accretion, which is gravitationally-driven mass transfer onto a compact object. I will then review the major observational categories of accreting neutron star and black hole binaries, and discuss the derivation from the data of important physical parameters including spin, mass, radius, binary orbital elements and the surface magnetic field strength and equation of state for neutron stars. Finally, I will close with a brief look at some new evidence and predictions of relativistic effects seen in these systems. A glossary of frequently used astronomical jargon is included, as well as a short tutorial on the names of X-ray sources.

2 X-ray Emission Mechanisms

In this section, I review the different theoretical mechanisms which are believed to produce X-ray emission in systems containing either neutron stars or black holes. Non-gravitationally driven emission mechanisms are reviewed so that they can be contrasted with accretion, the primary gravitationally-driven mechanism that produces high-energy photons.

2.1 Rotationally Powered Pulsars

Rotationally powered pulsars were discovered by Jocelyn Bell and Anthony Hewish in 1964,[2] and recognized as rotating neutron stars in work by Gold.[3] They have been extensively studied at radio wavelengths, where $\sim$ 1000 such objects are detected (for a comprehensive review, see *Pulsar Astronomy*[4]). The radio emissions are the result of a pulsar wind of relativistic plasma, powered by the loss of rotational kinetic energy as the pulsar's spin slows, and beamed along the open magnetic dipole field lines that are offset from the rotational axis of the star. The luminosity that is detected is consistent with the loss of rotational kinetic energy, $\dot{E} = I\omega\dot{\omega}$, where I is the moment of inertia of the object, and ω is its angular velocity.

At the highest gamma-ray energies, seven rotationally powered pulsars are seen. Figure 1 shows the multi-wavelength lightcurves of the seven known gamma-ray pulsars. Theoretical speculation as to the origin of the high-energy radiation and its phase relation to the emission at lower energies has settled into two main types of models: those in which the high-energy radiation is emitted from the polar caps (*i.e.*, where the open magnetic field lines emanate[5]) or those in which it arises from the "outer gaps", where the last closed field line intersects the speed of light cylinder[6] (see Figure 2).

A very successful recent outer gap model by Romani and Yadigaroglu[7] provides calculations of the rotating neutron star's magnetosphere and accounts for the origins of the different types of emission and their phase relationships, as a function of only two important parameters: the angle between the rotation axis and the magnetic dipole axis, and the angle to our line-of-sight. Figure 3 shows a typical calculation from their work.

In all cases, the neutron stars which have been carefully studied have masses consistent with 1.4 $M_\odot$, radii of about 10 km, and therefore moments of inertia $I = 10^{45}$ g cm^2. Their spin periods vary from milliseconds to tens of seconds. Changes in the pulse period can be used to derive the pulsar's spin-down age as well as its magnetic field. The spin-down age is defined as:

$$\tau = \frac{P}{2\dot{P}} \tag{1}$$

while the magnetic field can be found from:

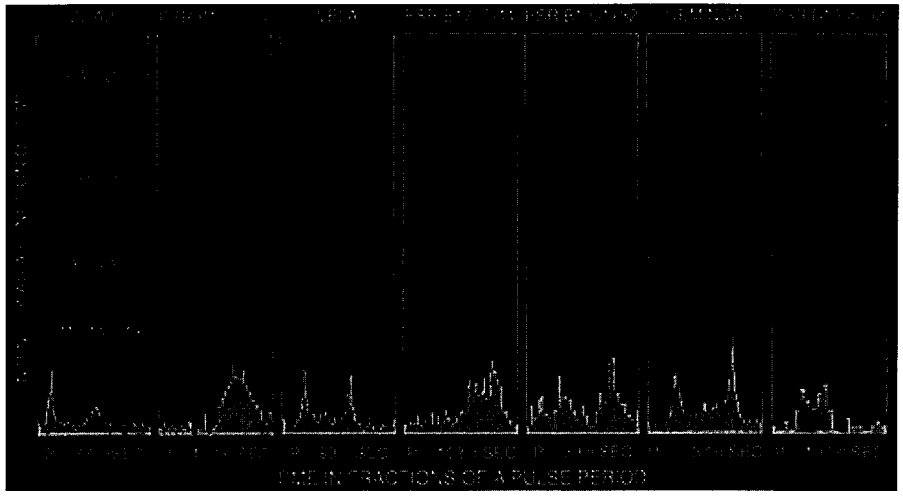

Figure 1: Multi-wavelength lightcurves showing the emission as a function of pulse phase for the seven rotational powered neutron star pulsars which are detected by the EGRET experiment on board NASA's Compton Gamma-ray Observatory.[8]

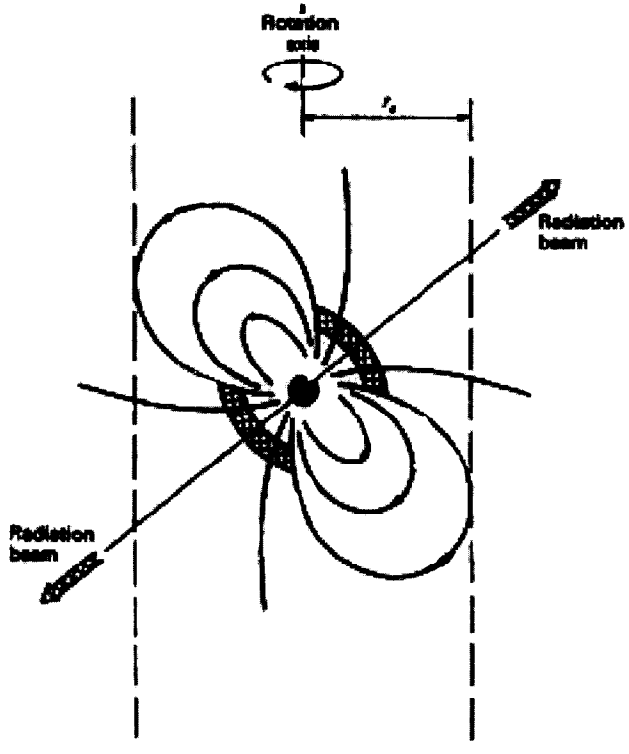

Figure 2: A schematic showing the relationship between the spin and magnetic field axes for a rotating neutron star. The polar caps are the cross hatched regions. The outer gaps are the portions of the outermost closed field lines which extend from the polar cap to the speed of light cylinder, which is denoted by the dashed lines.[4]

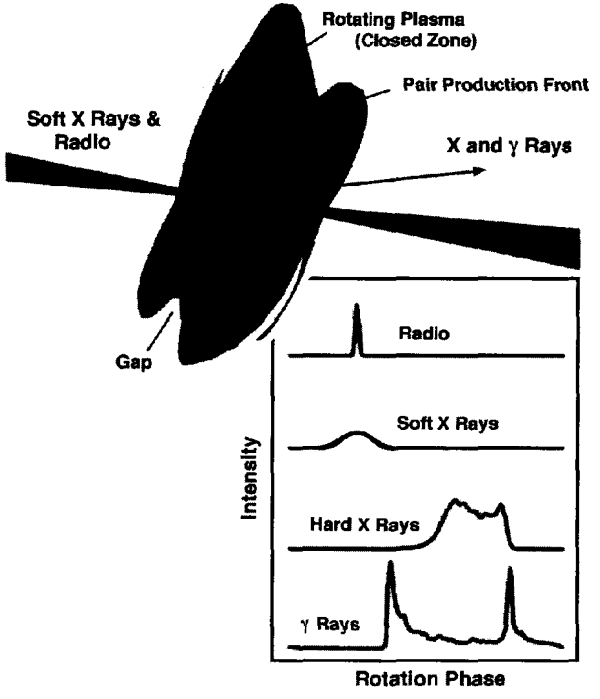

Figure 3: Neutron star magnetosphere showing the correlation between emitting surfaces and wavelength as predicted by the outer gap model calculations of Romani and Yadigaroglu.[7]

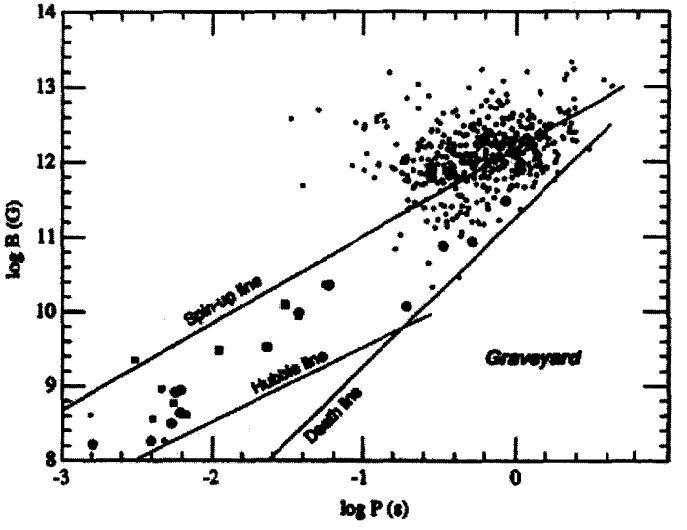

Figure 4: Derived magnetic fields for many radio pulsars as a function of pulse period.[9]

$$B = 3.2 \times 10^{19} \, (\dot{P}P)^{1/2} \text{ Gauss.} \quad (2)$$

Figure 4 shows the spin periods for many of the well-studied radio pulsars as a function of their derived magnetic field strengths. The millisecond pulsars are believed to be "recycled", *i.e.*, spun up via accretion from a companion star, after a previous evolutionary phase in which they were spinning down as isolated pulsars. The spin-up line noted on the figure indicates the minimum period that would result from accretion at the Eddington limit, while the Hubble line corresponds to a spin-down age roughly as old as the universe, or $\sim 10^{10}$ years. The death line delimits the region where the polar cap voltage is so low that pulsations are likely to switch off, and thus will not be observable.

Although X-ray luminosities in these systems can be quite high, often comparable to those produced by accretion, the steady spindown of the pulse period is in marked contrast to the much more variable spin rate behavior in the accret-

ing binaries. And, for those rotationally powered neutron stars which are not in binaries, no companion stars can be detected.

2.2 Shock Emission From Pulsar Winds

Recently, several radio pulsars have been found with non-compact companion stars. These systems, the "recycled" pulsars, are rotating much more rapidly than conventional non-binary radio pulsars, having been spun up by accretion from their companions. They are believed to be much older systems, with magnetic fields that have decayed to $\sim 10^8$ Gauss.

Binary radio pulsars are seen with different types of non-compact companions. First to be discovered at high energies were very small systems, where the effects of the pulsar wind on the companion's outer layers caused the rapid ablation of the small star. For example, in the case of the "Black Widow" pulsar[10,11] PSR 1957+20, the companion is only $\sim 0.02 M_\odot$, and is being "eaten" by the $\sim 10^{35}$ ergs s^{-1} wind from the 1.6 ms pulsar. Due to the shock-heating of the outer layers of the small star, about half of this emission occurs at higher energies (*i.e.*, X- and gamma-rays).

Cominsky, Roberts and Johnston[12] discovered X-ray emission from PSR B1259-63, a 69 ms radio pulsar[13] that orbits a Be-star (SS 2883). This unusual system has a 3.4 year, very eccentric orbit, and has now been observed throughout its orbital cycle. The high-energy emission seen from this system is most likely due to shock-heating of the Be-star's wind by that of the pulsar.[14,15] Recent work has shown that the power-law spectral index of the high-energy emission remains almost constant throughout the long orbital cycle; it is only the normalization that changes as the two stars separate.[16] Figure 5 compares the energy spectrum seen at periastron (closest approach) to that at apastron (furthest separation) in the PSR B1259-63 system. The X-ray luminosity seen in this system varies by a factor of ten from $\sim 10^{33} - 10^{34}$ ergs s^{-1} as the neutron star travels from apastron to periastron.

2.3 Magnetars (Soft Gamma Repeaters)

The presence of extremely intense magnetic fields in a class of isolated neutron stars known as magnetars, and their association with an observational class of objects known as the Soft Gamma-ray Repeaters (SGR) has been suggested[17,18]

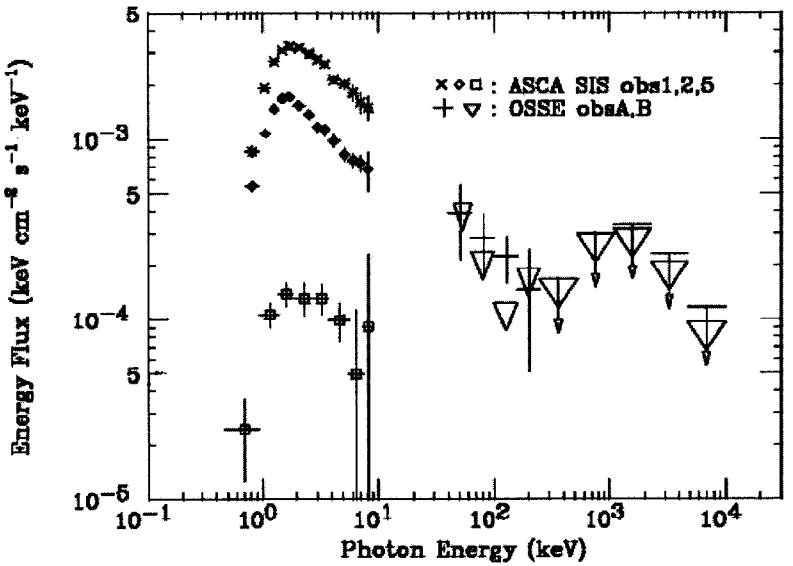

Figure 5: The spectrum of the Be-binary pulsar system PSR B1259-63 showing the changes in intensity as a function of the separation between the two stars. The two upper curves at low energies are from periastron observations,[15] while the lower curve is at apastron. X-ray emission up to 100 keV is detectable at periastron,[19] but apastron observations have resulted in only upper limits.[16]

by Thompson and Duncan. Unlike conventional gamma-ray bursts, the SGRs show repeated bursts of soft gamma-rays over many years from the same location. There are now[20] four SGR: three in our galaxy and one in the Large Magellanic Cloud. All are associated with young supernova remnants. The key difference between magnetars and rotationally powered pulsars is that the energy source powering the magnetars is derived from the rapidly decaying magnetic field, which heats the core and surface of the star.

As an example, detailed observations[21] of SGR1806-20 have shown 7.47 second hard X-ray pulsations with a spindown rate of 2.6×10^{-3} yr^{-1}, indicating a pulsar spindown age of $\sim$ 1500 – 8000 years, and a magnetic field of $\sim 2 - 8 \times 10^{14}$ Gauss. Peak burst fluences seen from SGR1806-20 are $\sim 10^{41}$ ergs s^{-1}, $\sim 10^3$ times the Eddington limit. These super-Eddington luminosities are possible because of the magnetic suppression of the Thomson cross-section for electron scattering. Quiescent X-ray luminosities following the bursts are $\sim 10^{35} - 10^{36}$ ergs s^{-1}, and are modulated at the neutron star spin period. Bursts from SGRs are easily distinguished from X-ray bursts and other gamma-ray bursts: SGR blackbody burst temperatures of 9 keV are about three times the highest temperatures seen in thermonuclear (Type I) X-ray bursts, but they are still much softer than non-repeating gamma-ray bursts.

In the magnetar models,[17,18] the sudden cracking of the neutron star crust leads to a rapid injection of Alfvén waves into the magnetosphere, particle acceleration and the formation of a optically thick pair plasma. Magnetic confinement of this plasma can produce the observed spectral similarities between bursts of greatly varying fluence. The repeated bursts from these objects are indications of starquakes caused by magnetic stresses in the neutron star crust.

2.4 Accretion In Neutron Star and Black Hole Binaries

In accreting X-ray binaries, the X-ray luminosity originates in $\sim 10^7 - 10^8$ K plasma near the neutron star's surface or from the inner accretion disk around the compact object. Accretion is extremely efficient; it liberates approximately 200 MeV per nucleon, compared to only 7 MeV per nucleon for the process of fusing hydrogen into helium. The accretion luminosity observed is given by:

$$L_{accr} = \frac{\eta\, G\dot{M}M}{R} \sim 1.2 \times 10^{38}\, \eta \text{ ergs s}^{-1} \qquad (3)$$

assuming that $M = 1.4$ M$_\odot$, $R = 10$ km, $\dot{M} = 10^{-8}$ M$_\odot$ yr^{-1}, and where η is an efficiency factor for the conversion of gravitational potential energy into radiated luminosity. The efficiency differs for neutron stars, black holes, and the assumed General Relativistic metric. Typical accretion luminosities observed in these systems vary from $10^{36} - 10^{38}$ ergs s^{-1}. Comprehensive references for this section can be found in *X-ray Binaries*[22] and *Accretion Power in Astrophysics.*[23]

The inner accretion flow occurs in a region of strong field gravity. For example, the potential well of a neutron star is 0.2 c^2 at 10 km for 1.4 M$_\odot$, and the characteristic velocity of the material in this region, $(\frac{GM}{R})^{1/2} \sim$0.5c.

In studying this inner accretion flow, one must take into account the very rapid dynamical timescales for matter to move through the emitting region:

$$\tau_{dyn} = (\frac{r^3}{G\,M})^{1/2}. \qquad (4)$$

This is about 0.1 ms for matter at $r = 10$ km, and 2 ms at $r = 100$ km. The typical orbital period of circulating matter,

$$P_{orb} = 2\pi\tau_{dyn} \sim 1 \text{ ms}. \qquad (5)$$

The two main accretion mechanisms are Roche lobe overflow, which most often occurs in low-mass binaries, and stellar wind capture, which is common for high-mass binaries with super-giant companions. A third mechanism for the initiation of mass transfer is often seen in systems with Be-star companions, as they are known to spontaneously eject matter in their equatorial regions due to their rapid rotation (even when they are not in binaries with compact objects).

2.4.1 Roche-lobe Overflow

Figure 6 shows the geometry for Roche lobe overflow. In this figure, the Roche lobe equipotential surface resembles a figure "8". The companion star completely fills its Roche lobe as the star evolves, and material in its expanding envelope is transferred through the inner Lagrangian (crossover) point to the vicinity of the compact object.

The compact object does not fill its Roche lobe; rather the accreted material swirls around it, interacting viscously to form an accretion disk (with a typical radius $R_{disk} \approx 0.8 R_{lobe}$). The intersection point of the incident stream with the

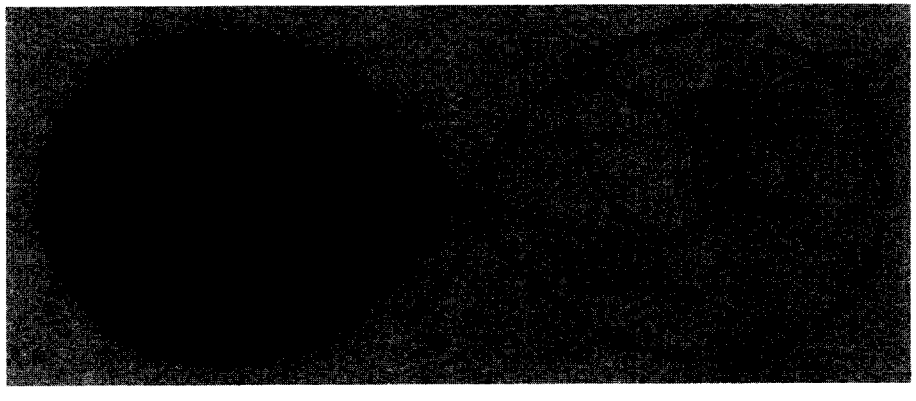

Figure 6: Roche lobe geometry, showing the incident mass stream through the inner Lagrangian point and the intersection of the returning stream with the newly arriving material. The low mass companion on the left hand side completely fills its Roche lobe, while the position of the compact object is denoted by a plus sign (+) inside the right hand lobe.[24]

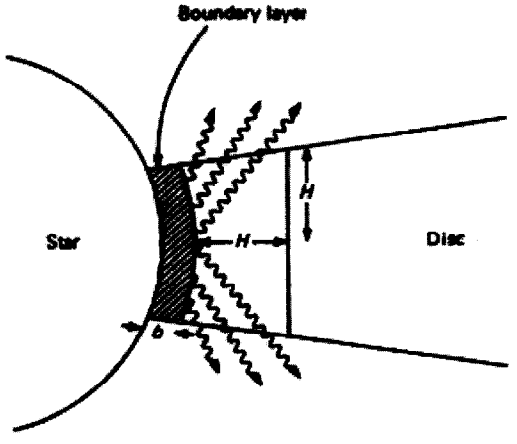

Figure 7: Accretion in a weak ($\sim 10^8$ Gauss) magnetic field. Note that the accretion disk extends to the neutron star surface.[23]

returning stream is a region of great turbulence, which can have interesting observational properties.

If the magnetic field of an accreting neutron star is relatively weak ($\sim 10^8$ Gauss), the accretion disk can extend all the way to its surface. The material then shocks to make a boundary layer, which radiates at X-ray wavelengths. This is illustrated in Figure 7.

For the much stronger magnetic fields (B $\sim 10^{12}$ Gauss) which are characteristic of pulsars, any accretion disk which is present can extend only to the surface of the magnetosphere. Matter must then travel along the field lines to the vicinity of the polar cap. The infalling material then shocks above the polar cap, producing observable high-energy emission (see Figure 8).

2.4.2 Stellar Wind Capture

Figure 9 shows a typical scenario for accretion due to the capture of stellar wind material by a compact object. Early-type, massive companion stars evolve by radiating a wind of mostly hydrogen plasma at a rate of approximately 10^{-6} $M_\odot$ yr^{-1}. A small fraction of this wind, typically 1%, can be captured as it passes

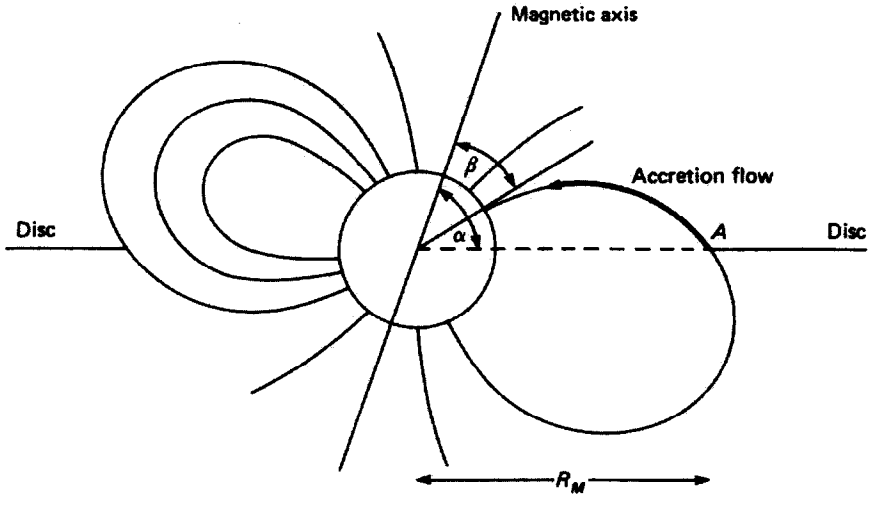

Figure 8: Accretion in a strong ($\sim 10^{12}$ Gauss) magnetic field. Note that the accretion disk is held off the neutron star surface by the centrifugal barrier formed by the rotating magnetosphere.[23]

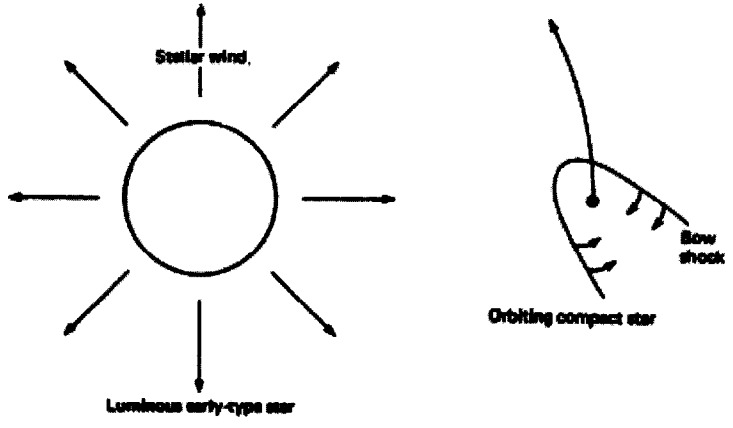

Figure 9: Accretion from a stellar wind.[23]

the compact object. A bow shock forms around the compact object, which can produce observable X-ray emission.[24]

2.5 Thermonuclear Reactions

As the matter accretes onto the neutron star surface, it settles into layers in which different elements undergo thermonuclear burning. Figure 10 illustrates the typical shell structure for neutron stars with relatively weak magnetic fields. In this case, the accretion flow can spread out over the entire neutron star surface, rather than being confined to the polar cap region by a much stronger magnetic field (as in the case for pulsars).

Following the discovery[25,26] of X-ray bursts in 1976, considerable theoretical work was done to account for the luminosity and spectral profiles of these sporadically occurring events. It is now well established that X-ray bursts are due to unstable thermonuclear burning in the surface layers of neutron stars.[27,28]

Three nuclear burning regimes have been defined, based on the mass accretion rate onto the neutron star surface.[29] For accretion rates in excess of 2.6×10^{-8} $M_\odot$ yr^{-1}, both the hydrogen and helium shells will burn stably; thus

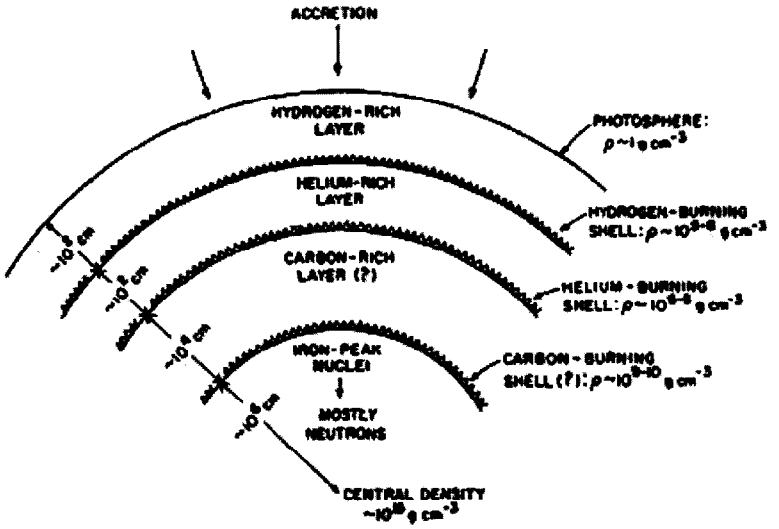

Figure 10: *Structure of a neutron star, showing the different elemental burning shells.*[30]

no bursts are seen. This is supported by considerable observational data in which the bursts are seen to grow weaker and then stop as the underlying, persistent, accretion-driven luminosity increases. For accretion rates between 2.6×10^{-8} $M_\odot$ yr^{-1} and 2×10^{-10} $M_\odot$ yr^{-1}, helium burns unstably, and runaway reactions cause helium flashes. Below about 2×10^{-10} $M_\odot$ yr^{-1}, hydrogen burns unstably, resulting in hydrogen flashes.

3 Accreting X-ray Binaries

In this section, I review the common characteristics of the major observational groups of neutron star and black hole binaries in which X-rays are produced by accretion onto the compact object.

3.1 X-ray Binary Pulsars

The primary distinguishing characteristic of X-ray binary pulsars is their extremely intense magnetic field, typically $\sim 10^{12}$ Gauss, which confines the bulk of the X-ray emission to the polar cap region. The offset magnetic dipole in these systems produces a unique pulse profile as the neutron star rotates on its spin axis. Typical pulse profiles are shown in Figure 11. Note that the pulse profile is quite variable as a function of energy. Although not totally understood, differences in pulse profile shape can be attributed to a combination of differences in viewing angle to the system, magnetic field strength, offset dipole angle and magnetic opacities along the line of sight.

There are over 30 well studied X-ray binary pulsar systems in our Galaxy. Their spin periods range from 0.025 to 840 seconds, and they are in orbits with binary periods ranging from 0.029 to 187.5 days.[31,32] Companion stars in these systems span the widest range of possible types, from stars much less massive than our Sun to supergiants. A prominent sub-group among the X-ray binary pulsars has Be-star companions. These systems tend to be in wider, often eccentric orbits and to show transient episodes of accretion, most probably triggered by sudden mass outflows by the Be-companion. Typical X-ray luminosities for these systems range from $10^{36} - 10^{38}$ ergs s^{-1}.

Studies of the relation between the spin and orbital periods in these systems have led to a correlation in only one type of sub-group, the Be-companion systems.

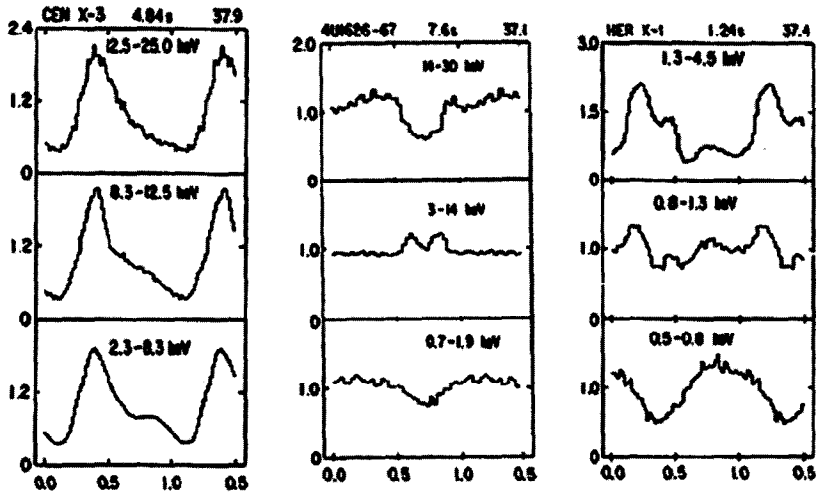

Figure 11: Pulse profiles as a function of phase and energy for three different X-ray binary pulsars.[33]

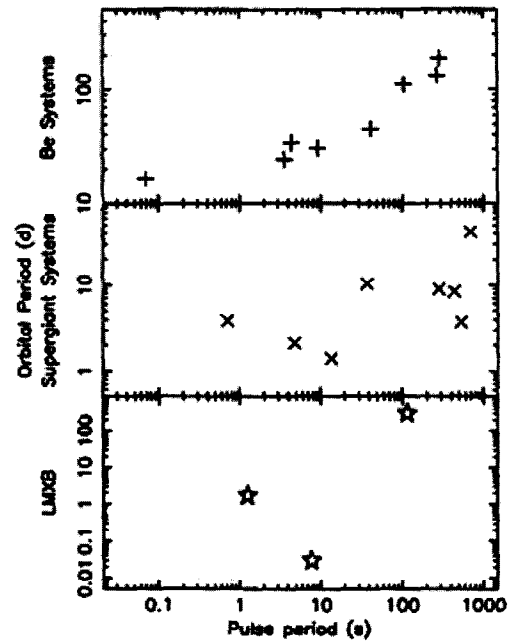

Figure 12: Orbital period as a function of pulse period for different types of accreting x-ray binaries. Note the linear relation for the Be-star systems.[31]

As can be seen in Figure 12, there is little correlation in the low-mass (Roche lobe overflow) or supergiant (stellar wind capture) systems. The roughly linear correlation in the Be-companion systems (often called the Corbet relation[34]) is taken as evidence that these systems have reached a rough equilibrium between the spin period and the orbital separation.

3.2 X-ray Bursters

Because of the presence of X-ray bursts, the magnetic field in these systems is believed to be $\sim 10^8$ Gauss. Models have shown that higher field strengths quench the bursting behavior, by narrowly focusing the accretion onto the polar cap

region, and thus greatly raising the local accretion rate (and the observed luminosity) to the range in which nuclear burning is stable.[35] Accretion occurs over a greater portion of the surface area in neutron stars with relatively weak fields, although the uneven channeling of accreted matter by the flow from the accretion disk can lead to hot spots which trigger the flashes, and to continuous low level fluctuations in the burning rate which can propagate around the star, producing the so-called "rings of fire".[36]

There are over 15 well-studied[37] bursting systems; all have low-mass companions, and most are located either in globular clusters or near the center of our Galaxy. These positional associations have led to the belief that X-ray bursters are an older population of object than the pulsars. Although their magnetic fields may once have been strong enough to cause pulsation, it is possible that the fields have decayed away in the intervening $\sim 10^{10}$ years. Typical luminosities for the persistent, accretion-driven emission in these systems are $\sim 10^{36}$ ergs s^{-1}, while the burst peaks are often about 100 times as luminous.

Orbital periods in these systems have been determined with high confidence using X-ray data in the two systems which exhibit X-ray eclipses. In 1981, Cominsky and Wood[38] discovered 15 minute long eclipses, which recur every 7.1 hours, in the transient X-ray burst source MXB 1659-29. Later observations of the source EXO 0748-676 showed that it too had X-ray eclipses.[39] All of the orbital periods for the other bursters, however, have been derived from quasi-regularly occurring X-ray dips in intensity due to the turbulent area of the gas stream blocking the line of sight, or by optical observations of intensity modulation due to X-ray heating of the companion star and/or accretion disk. Known orbital periods in the bursting systems vary from 0.19 to 398 hours.

X-ray bursts are well described by thermal black-body spectra,[40] in which the radius is roughly constant as the temperature increases to around 3×10^7 K and then cools until the resulting luminosity is undetectable below the background (most of which stems from the persistent accretion luminosity). Some bursts are accompanied by a sharp jump in radius at the beginning,[41] before settling down to the $\sim$ 10 km radii more typical of neutron stars. This radius expansion is evidence that the burst flux has reached the Eddington limit (roughly 10^{38} ergs s^{-1}), and that the photosphere of the neutron star has temporarily inflated due to excess radiation pressure. Figure 13 shows a black-body fit to four energy channels of X-ray data for a burst from a globular cluster source, in which radius expansion is present. The radius expansion at the peaks of some bursts allows one to use the Eddington limit to derive distances to the bursters, *i.e.*, they act as "standard candles". Distances derived in this manner are consistent with those derived from other means, *e.g.*, by analyzing the constituents of the globular clusters, or by noting the distribution of sources around the Galactic center.[42]

The recent discovery[43] of quasi-periodic oscillations (QPO) at a period of about 3 ms (or half that) within X-ray bursts themselves, has greatly intrigued the high-energy astrophysical community. Since the burst emission is a direct indication of conditions on the surface of the star, these QPO are taken as the first direct evidence of the neutron star's spin, and are perhaps the result of one or two hot spots of emission rapidly rotating with the star.

There is also a second type of X-ray bursting pattern - the so-called "Rapid" or Type II bursts, which, until recently, were only seen from one object, the Rapid Burster[44] (MXB 1730-335). This type of pattern, in which thousands of closely spaced, non-thermal bursts are observed daily, is attributed to instabilities in the neutron star's magnetosphere. Episodes of rapid bursting are transient, occurring for only $\sim$months out of $\sim$years. However, the Rapid Burster also shows Type I, or thermonuclear flash bursts on occasion, indicating that the neutron star is accreting matter, although very unsteadily. The rapid bursts repeat in a pattern that has been likened to that of a Relaxation Oscillator: the fluence in each burst is proportional to the waiting time to the next burst.[45] This "$E - \Delta t$" relationship is illustrated in Figure 14.

In 1996, another object (GRO J1744-28) was discovered that displays a rapid bursting pattern with inter-burst intervals as short as $\sim$minutes.[46] However, unlike the Rapid Burster, GRO 1744-28 also pulses with regular 0.47 second pulsations.[47] The observed spinup and Doppler shifts of these pulses during its transient outburst indicates that it is accreting from a low-mass binary companion. Magnetic field strength estimates for the pulsar are $\sim 3 \times 10^{11}$ Gauss.[48]

In 1998, 2.5 ms pulsations were discovered[32] from the transient source SAX J1808.4-3658. This remarkable system, the fastest accreting X-ray pulsar now known, is in a $\sim$ 2 hour binary orbit[49] with a companion star that has less mass than 0.1 $M_\odot$. SAX J1808.4-3658 also emits Type I X-ray bursts.[50] Magnetic field estimates[51] for the neutron star in this system are $\sim 10^8$ Gauss leading to the conclusion that this low-mass X-ray binary system is a progenitor to the recycled millisecond pulsars. GRO1744-28 may be a similar evolutionary "missing link".

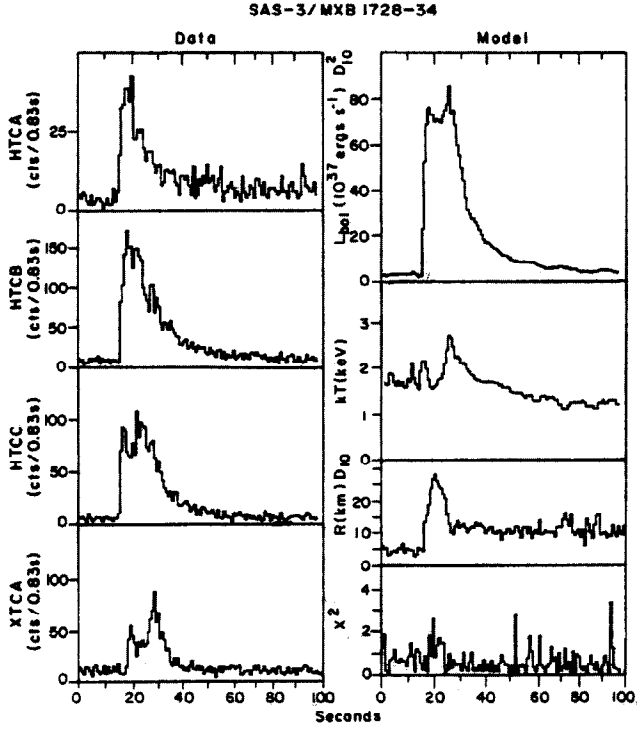

Figure 13: Blackbody fit for four X-ray energy channels. Note the jump in radius at the beginning of the burst as a result of Eddington-driven photospheric expansion.[52]

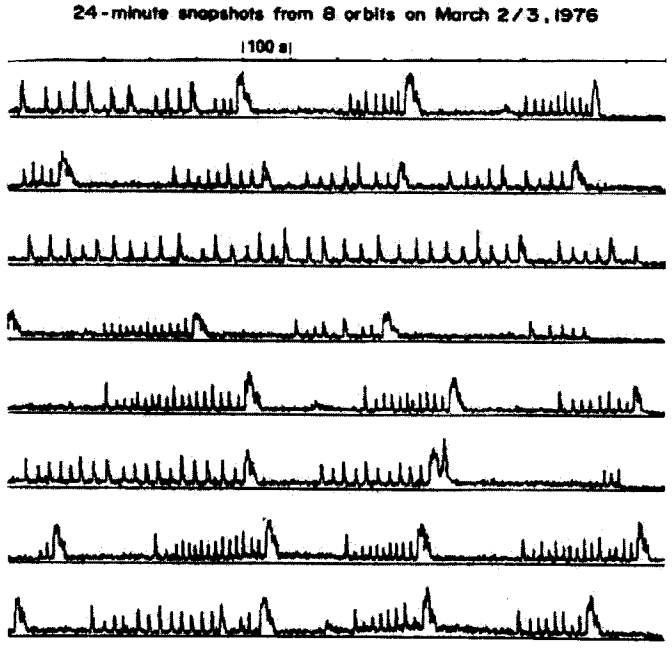

Figure 14: Type II bursts from the Rapid Burster, MXB 1730-335, showing the $E - \Delta t$ relationship, in which the fluence in a burst is proportional to the interval to the next burst.[53]

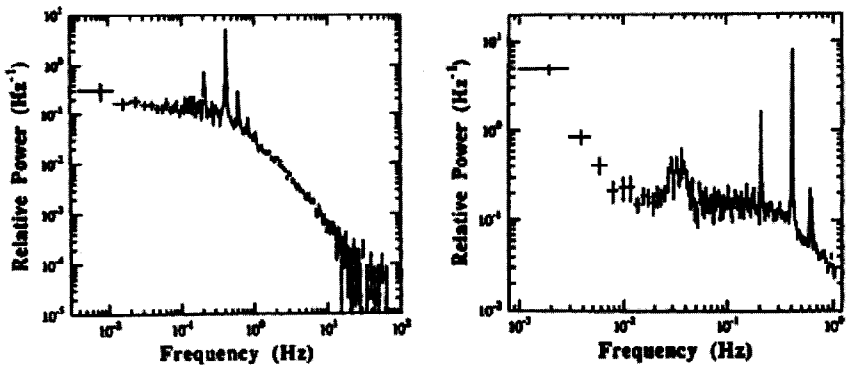

Figure 15: Power spectra from the X-ray binary pulsar Cen X-3 on two different occasions. Note that the spectrum on the right shows both the pulsing and QPO behavior, while the one on the left shows only the pulsing.[54]

3.3 Quasi-Periodic Oscillators

Unlike pulsars and bursters, quasi-periodically oscillating X-ray sources can be either neutron stars or black hole candidates.[55] Other QPO sources are the very luminous sources near the Galactic center, presumably neutron star binaries, which do not exhibit X-ray bursts as their mass accretion rate is too high. Both of the "microquasar" black hole candidates also show QPO.[56,57] Fourier spectra of pulsars often, but not always, exhibit QPO in addition to pulsations, which can be distinguished by the much-higher quality factors ($Q > 100,000$ vs. $100 - 1000$, see Figure 15).

When originally discovered[58] in observations using the EXOSAT observatory, the QPO ranged from 6 - 60 Hz. A typical example of QPO from a black hole candidate is shown in Figure 16. The most popular interpretation of the phenomena was the so-called "magnetospheric beat frequency" model.[59] In this model, the QPO emission arises from the beat between the Keplerian orbital frequency of matter circulating at the object's magnetosphere and the neutron star spin period. Many detailed studies were done of the QPO properties compared to the properties of the underlying persistent luminosity. Objects exhibiting QPO were

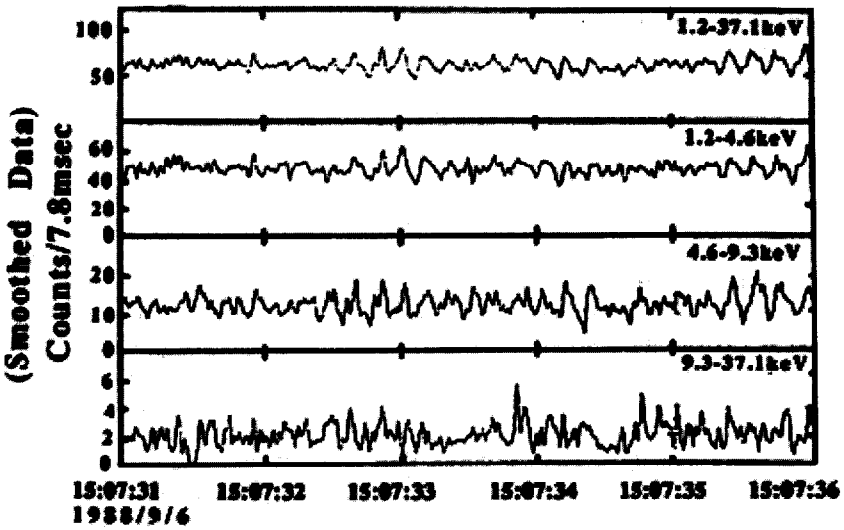

Figure 16: Time series from the black hole candidate GX 339-4, showing the 6 Hz quasi-periodic oscillations.[60]

classified as either "Z" or "atoll" sources,[61] depending on the pattern that they made in a plot of the normalized count rates in lower energy channels vs. those in higher energy channels, for a given intensity state ("color-color" diagram, see Figure 17). It is now established that the "Z" pattern is typical among the strong, non-bursting, non-pulsing galactic center sources, which have luminosities at approximately the Eddington limit, and magnetic fields of $\sim 10^9$ Gauss. In contrast, the "atoll" pattern is characteristic of the X-ray bursters, with luminosities of only about 1% of Eddington, and magnetic field strengths about ten times lower.

With the launch of the Rossi X-ray Timing Explorer (RXTE) at the end of 1995, a new observational window was opened, with both higher time resolution and greater sensitivity. Almost immediately, QPO began to be detected in the kHz range.[62] To date, there are at least 13 low-mass X-ray binaries which show QPO in the range 300-1200 Hz. Of these 13 sources, 4 are "Z" sources, and 9 are "atoll" sources. The kHz QPO, unlike the original QPO, typically occur in

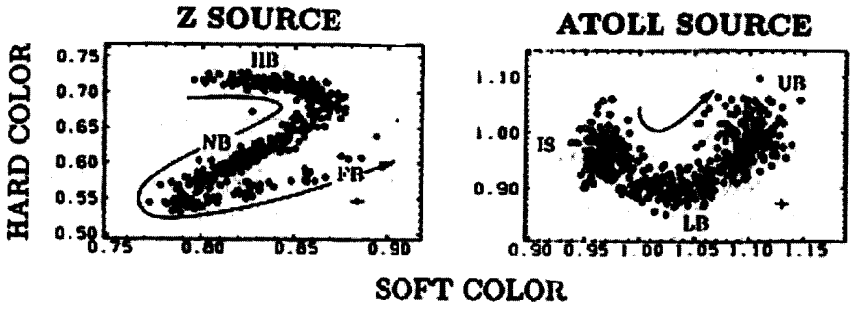

Figure 17: A comparison of the color-color diagrams for a Z vs. an atoll QPO source.[61]

pairs, known as the "twin peaks". Initial analysis of the frequency spacing of these peaks indicated that their separation was almost constant, at about 300 Hz. And, amazingly enough, this seemed to match the frequency (or half that, assuming that the bursts can emanate from two hot spots) seen in the bursts from the atoll sources.[63]

While the original magnetospheric beat frequency model can not be applied to the kHz QPO, it has been retooled to account for these new observations.[43] The frequency of the upper twin peak has now been associated with the Keplerian orbital frequency of matter in the inner accretion disk, perhaps just outside the marginally stable orbit or at the sonic point.[64] The lower twin peak then is interpreted as the beat frequency between this Keplerian orbital frequency and the neutron star's spin frequency. The 300 Hz difference frequency, which is often seen in the X-ray bursts, is that of the neutron star spin.

New data, however, and data from the strongest, and hence best signal-to-noise source (Sco X-1) have cast some doubt on this tidy interpretation. In Sco X-1, the value of the difference frequency is observed to be anticorrelated with the luminosity of the source.[65] It is not possible for the neutron star's spin to change on such rapid timescales, which leaves the door open for other possible models, such as those in which oscillating photon bubbles (PBO) in the accretion stream produce the QPO.[66] In addition, the claim of ~constant separation between the twin peaks in other, less luminous sources, may be an artifact of the statistics.[67] This is illustrated in Figure 18.

4 Physical Parameters of X-ray Binaries

In this section, I will review how X-ray data from Earth-orbiting satellites are used to determine the fundamental physical parameters of accreting neutron star and black hole binaries, and how these parameters change with time. Observations of compact X-ray sources provide information about the extreme conditions of temperature, density, magnetic field and strong gravity that are not available in earth-bound laboratory environments.

4.1 Neutron Star Spin

The spin of a neutron star is directly observable in Fourier analysis of the time series data obtained with sufficiently sensitive X-ray detectors. Extremely high-Q spikes ($> 100,000$) are seen in the power spectra of these objects, for even short stretches of data. For proportional counter detectors with areas in excess of about 1000 cm^2, individual pulses are easily seen, as pulsed fractions of the underlying accretion luminosity are typically $\sim 30\%$. A typical power spectrum, from only ~ 30 minutes of data, and less than 500 cm^2 of detecting area is shown in Figure 19. The fundamental, and the first two harmonics of the 3.6 second period are easily seen in this power spectrum for the transient Be-star system, 4U0115+63.

Changes in the spin rate from neutron stars were long believed to be well described by accretion torque theory.[68,69] Systems with accretion disks were believed to be prograde, and hence should spin up as they received angular momentum from the accreted material. In this standard accretion torque theory, the relation between the observed spin period P, the luminosity L of the X-ray source (which measures the amount of transferred matter) and the predicted change in the spin period $\dot{P}$ are related by:

$$\dot{P} \propto P^2 \, L^{6/7} \tag{6}$$

As shown in Figure 20, the theory appears to fit the long term trend towards spin up found in many systems. In this figure, the different curves refer to different

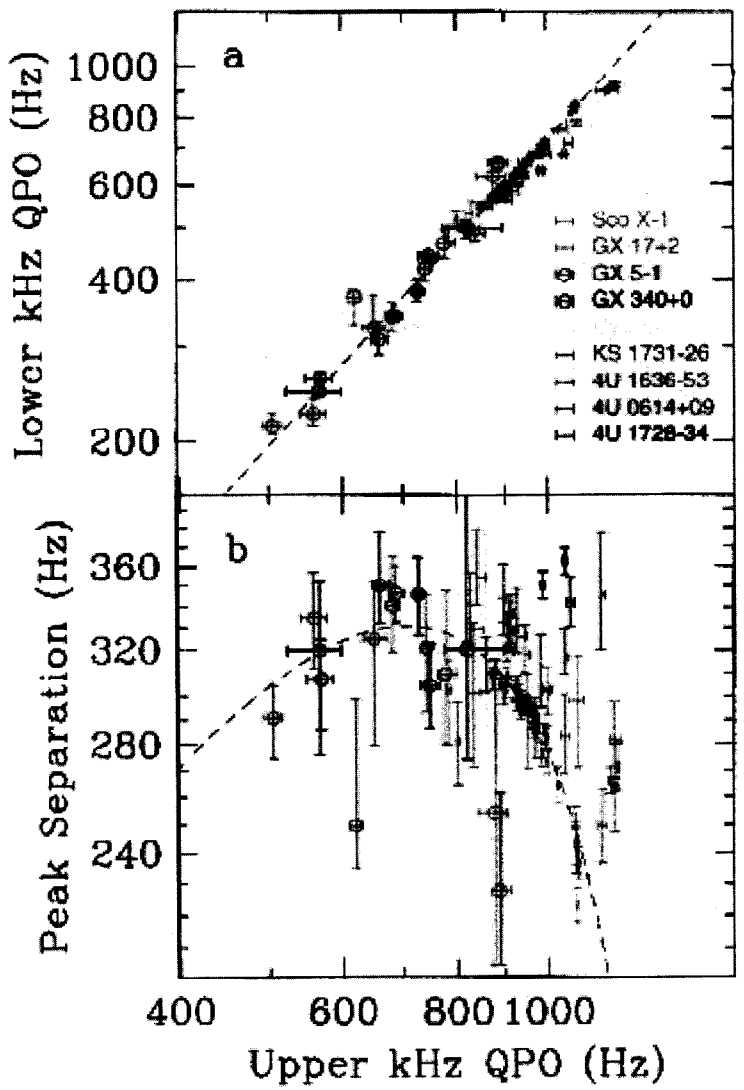

Figure 18: The frequency of the upper kHz QPO peak vs. the frequency of the lower QPO peak for many sources. Note that the peak t necessarily constant as a function of the upper kHz QPO peak frequency. This makes it difficult to associate the peak separation with the neutron star spin.[67]

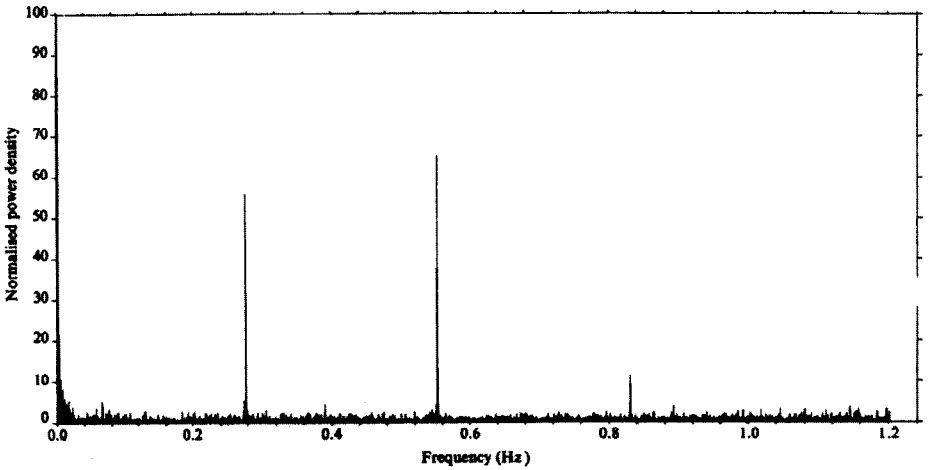

Fig. 1 Power density spectrum for 4U0115+63. The data were obtained with the SAS 3 Y-axis detectors during one satellite orbit near 10.5 January 1978 (UT).

Figure 19: Power spectrum of a typical X-ray binary pulsar, 4U0115+63, using data from SAS-3. The fundamental, at $P = 3.6$ s is easily seen, as well as the first two harmonics.[70]

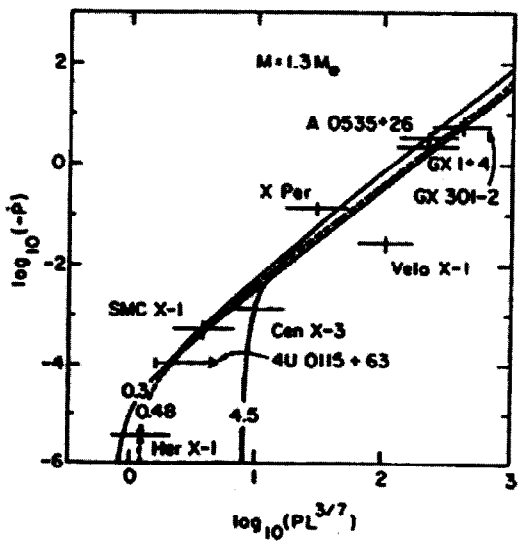

Figure 20: Period vs. luminosity according to standard accretion torque theory.[68]

values of the assumed magnetic moment μ in units of 10^{30} Gauss cm^3. Data for this figure were obtained by taking snapshots of the pulse period of the individual sources at irregular intervals, with separations of months, for up to 10 years for some sources.

However, recent continuous pulse monitoring by the BATSE experiment on board the Compton Gamma-ray Observatory (CGRO) has shown that the simple accretion torque picture must be replaced with something far more complex.[71] Long term (~years) spin up trends, based on coarsely sampled data, are the result of alternating intervals of spin up and spin down. Detailed analysis of the two different states has shown that the distribution of torques is roughly bimodal, with the spin up torque slightly larger than the typical spin down torque. In some systems, the torque changes sign as often as $\sim 10 - 100$ days, while in others, the reversal is every $10 - 20$ years. These observations have been interpreted as evidence that the accretion disks in these system may be alternating between episodes of prograde and retrograde rotation.[72] Although this type of behavior can be seen in numerical simulations of wind-fed systems, it seems difficult to achieve in systems that are accreting via Roche lobe overflow.

In transient systems, however, the standard accretion torque theory seems to hold, at least for the much shorter timescales of the outbursts. During outbursts, accretion occurs, and the neutron stars spin up in good agreement with accretion torque theory. Between outbursts, when little or no accretion occurs, the neutron stars spin down again.

4.2 Neutron Star Magnetic Field

The strength of the magnetic field on the surfaces of neutron stars can be directly inferred from the presence of cyclotron scattering resonance features in the energy spectra of (at least nine) X-ray pulsars. Figure 21 shows a comparison between the spectra of three X-ray pulsars with these features and one without. The magnetic field strength can be derived[73] as follows:

$$E = \frac{ehB}{2\pi m_e}(2n+1) + \frac{p_z^2}{2m_e} \tag{7}$$

where E is the true cyclotron line energy, B is the magnetic field strength at the neutron star surface, p_z is the angular momentum along B, and n is the quantum number specifying the Landau level. For the first cyclotron line, the electrons transit from $n = 1$ to the $n = 0$ level. Neglecting changes in the longitudinal angular momentum, we therefore find that:

$$E = 2\mu_B B \tag{8}$$

where μ_B is the Bohr magneton. However, the observed absorption energy E_{obs} is related to the true energy E by the gravitational redshift factor:

$$E_{obs} = \frac{E}{1+z}, \tag{9}$$

where the redshift z is defined as:

$$1 + z = (1 - \frac{2GM}{Rc^2})^{-1/2} \tag{10}$$

and has typical values of $z \sim 0.3$. This yields a relation between the true magnetic field strength B and the observed line energy E_{obs}:

$$B = 1.12 \times 10^{12} (\frac{E_{obs}}{10 \text{ keV}}) (\frac{1+z}{1.3}) \text{ Gauss} \quad (11)$$

Cyclotron scattering resonance line features are observed between 7 and 40 keV, which corresponds to a range of surface magnetic field strengths between $(0.8 - 4.4) \times 10^{12}$ Gauss.

4.3 Neutron Star Radius

The most direct measurements of the radii of neutron stars are derived from observations of X-ray bursts in globular cluster sources, to which the distances can be determined by independent methods. These black-body spectral fits yield photospheric radii of $10 - 20$ km, consistent with the range expected for likely equations of state. However, significant uncertainties remain: there may be deviations from pure black-body spectra due to the effects of the neutron's star photosphere; the radius expansion seen in many of the bursts indicates that the observed radiation may not be emitted directly from the neutron star's surface; and the analysis technique of subtracting the persistent accretion luminosity prior to fitting the burst spectrum may introduce additional uncertainties.[37]

The more recent observations of kHz QPO in many of the accreting X-ray binaries have provided a new method for the radius estimation for neutron stars.[74,75,76] The highest observed QPO frequency is ~ 1100 Hz: this is seen in at least 8 systems. The ubiquitous nature of this highest frequency argues that it is associated with the maximum predicted orbital frequency, found at the disk termination radius. For most systems with weak magnetic fields, this radius should be approximately equal to the marginally stable orbit r_{ms}, given an assumed General Relativistic metric:

$$r_{ms} = \frac{\alpha G M}{c^2}. \quad (12)$$

In the above equation, α is a factor which varies from 1 for a maximally prograde Kerr (rotating) system, to 9 for an extreme retrograde Kerr system. For the non-rotating Schwarzschild metric, $\alpha = 6$. Therefore, for the canonical 1.4 $M_\odot$ neutron star (in a Schwarzschild metric), the assumption that the neutron star radius must be inside r_{ms} sets a firm limit of 12 km on its radius.

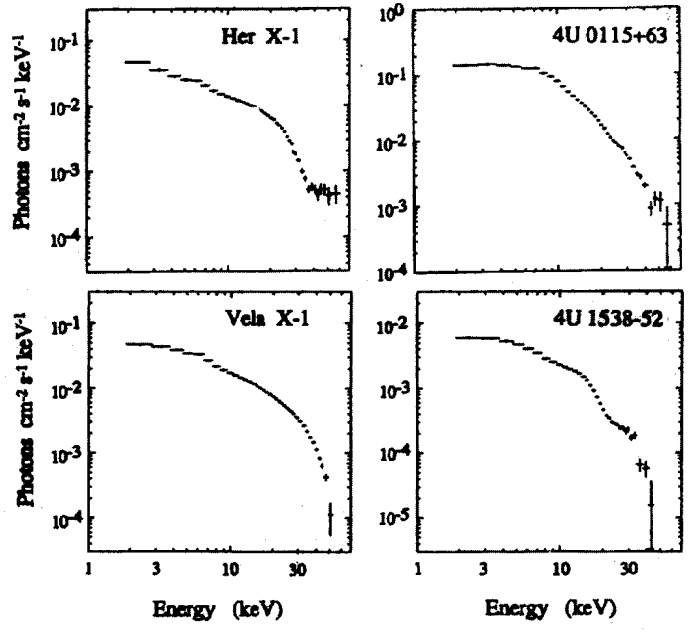

Figure 21: Energy spectra for four binary X-ray pulsars using data from the *Ginga* satellite. Three show cyclotron lines: Her X-1 at ~ 35 keV, 4U0115+63 at 12 and 23 keV, and 4U1538-52 at 21 keV. Vela X-1, in the bottom left hand panel, does not. The feature near 6.7 keV is the Iron K line.[31]

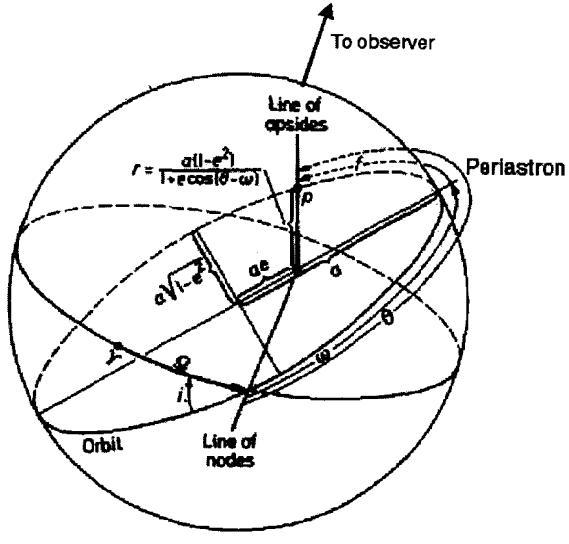

Figure 22: The definition of the orbital elements. The semi-major axis (a), and the eccentricity (e) can clearly be seen on the figure. The longitude of periastron (ω) is the angular distance between the plane normal to the observer's line of sight and the periastron point along the orbit. The inclination angle (i), is the angular distance between the plane of the orbit and the plane normal to the observer's line of sight.[77]

4.4 Orbital Determination in X-ray Binaries

The five observational parameters which uniquely describe a binary orbit are shown in Figure 22. They are: a, the amplitude of the semi-major axis; T, the time of periastron passage; ω, the longitude of periastron; e the eccentricity; and i, the inclination angle of the orbit to our line-of-sight. The accuracy to which these parameters can be determined has considerable dynamic range and depends on the type of observational data which are available for a given system.

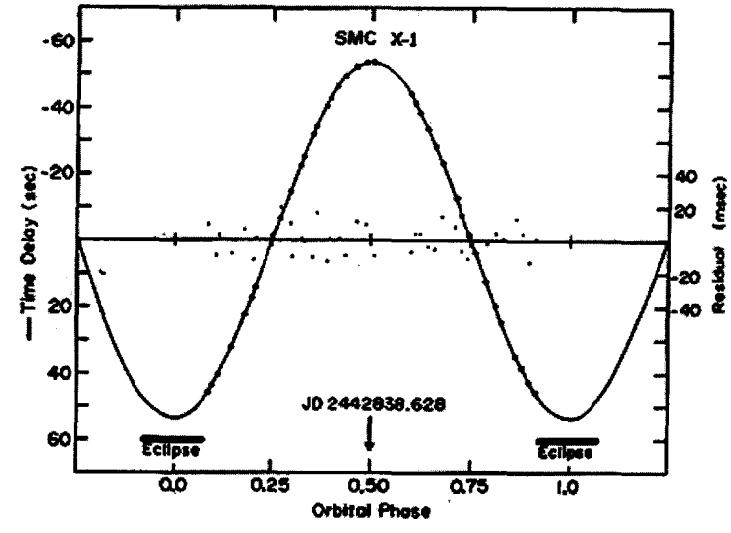

Figure 23: Doppler orbital fit for SMC X-1, a eclipsing, circular binary.[78]

4.4.1 X-ray Pulsars

Analysis of Doppler shifted pulses in X-ray binaries is used in the most accurate determination of the five orbital elements.[79] Fitting either the Doppler delays or the pulse arrival times to Kepler's equation together with additional pulse period derivative terms (to account for accretion torques) can yield results that are extremely accurate (uncertainties are typically less than 10^{-6}). Figure 23 shows an example of the orbital fit for a high-mass, eclipsing binary with a circular orbit (SMC X-1), while Figure 24 shows a Be-star transient pulsar in an eccentric orbit (4U0115+63). In both cases, Doppler delays of the order of 50 -100 seconds are seen, and residuals from the fits are ~tens of milliseconds. Figure 25 shows a summary of the orbital fits for 11 X-ray pulsars. The wide (and often eccentric) orbits seen in the Be-systems V0332+53, 2S1553-54, and 4U0115+63 contribute to the transient X-ray outbursts which are often seen in these binaries.

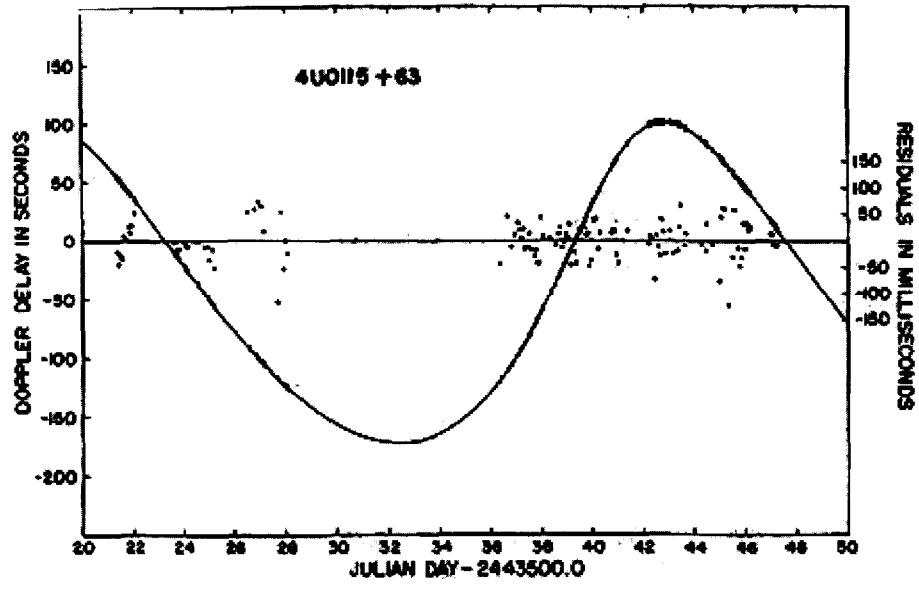

Figure 24: Doppler orbital fit for 4U0115+63, an eccentric, transient Be-star system. Note the Doppler curve is skewed by the eccentric nature of the orbit.[80]

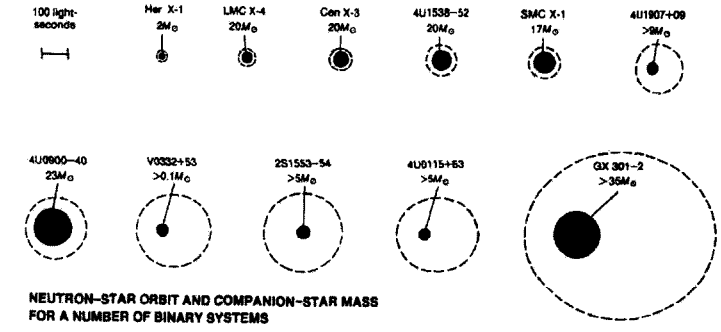

Figure 25: Comparison of the orbital dimensions for many of the X-ray binary pulsars. The five smallest systems show eclipses, as does 4U0900-40 (Vela X-1), which is in a slightly eccentric, but close orbit, with a supergiant companion. The wider, often eccentric systems with small companions on the bottom row contain Be-stars.[81]

4.4.2 Non-pulsing Low-mass X-ray Binaries

In contrast to the high-mass and/or pulsing X-ray binaries, there are only two low-mass X-ray binaries which show true X-ray eclipses by the companion star.[38,39] The orbital periods in these two systems can be determined to better than 10^{-8}, but the other four orbital elements cannot be well determined (although some information is available from optical observations). The two eclipsing sources and an additional 10 LMXBs show irregularly spaced modulations or fluctuations in X-ray intensity ("dips") that are attributed to obscuration by the gas stream from the companion star, as it joins the accretion disk. However, for the great majority of these sources, no defining orbital signatures can be observed in X-ray data. Optical modulation of the low-mass companion (or perhaps the X-ray heated accretion disk) has resulted in the majority of the orbital determinations in these types of systems, with correspondingly greater uncertainties.

The relative paucity of eclipsing low-mass X-ray binaries was explained in a classic paper by Milgrom.[82] Obscuration by the relatively large accretion disk prevents X-rays from being detected when the inclination of the binary is optimal for viewing X-ray eclipses by the companion star (*i.e.*, in the orbital plane). When the viewing angle begins to rise above the orbital plane, the companion star is so small that there are only a few systems in which eclipses will be seen. And even in these systems, the eclipses are very short, due to the grazing angle of the line-of-sight. This observational situation is depicted in Figure 26 and a summary of the orbits for many LMXBs in shown in Figure 27. Note that Her X-1 and 4U1626-67, both pulsars, have low-mass companions, as do several of the black hole candidates (represented in this figure by A0620-00). One of the two eclipsing[38] binaries, MXB 1659-29, is also shown in this figure.

4.4.3 Orbital Evolution

Changes in the period of the binary orbit have only been detected in a handful of X-ray binaries. In contrast to the Hulse-Taylor binary radio pulsar system,[83] the decay of X-ray binary orbits is not attributable to the emission of gravitational radiation. In the high-mass X-ray binary Cen X-3, successive eclipse timings over more than ten years were used by Kelley et al.[84] to show that the fractional change in the orbital period was decreasing by about 10^{-6} yr^{-1} (see Figure 28). This orbital decay is consistent with a loss of angular momentum from the system

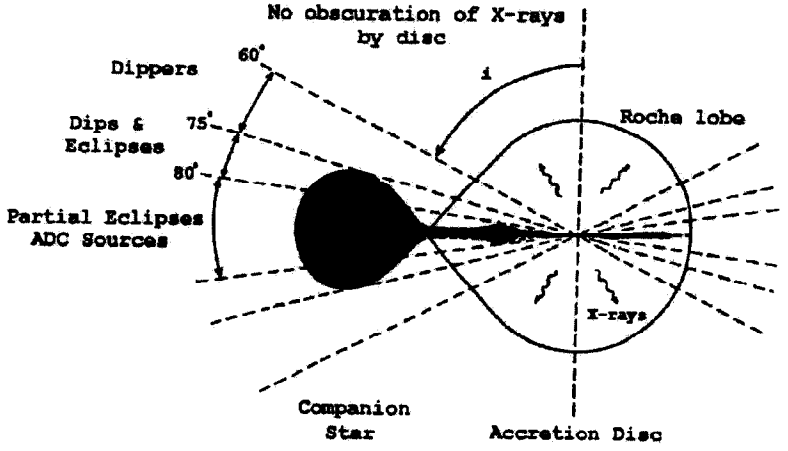

Figure 26: Observational properties of low-mass X-ray binaries as a function of line-of-sight angle to the orbital plane.[81]

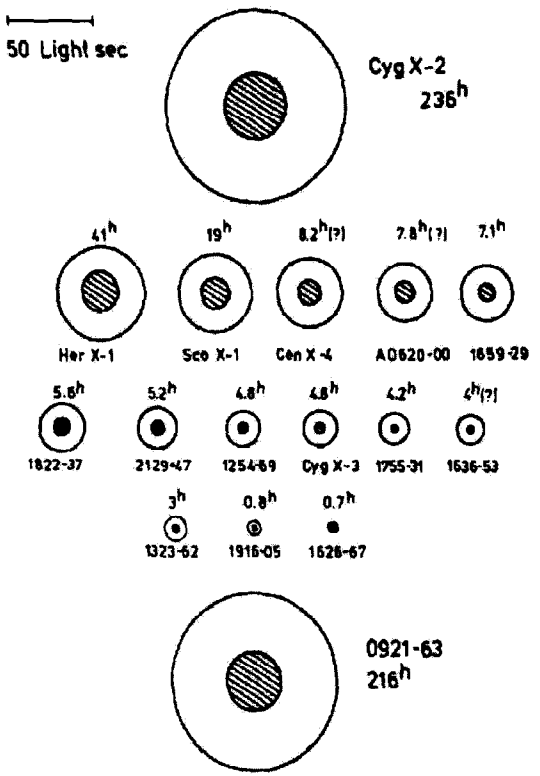

Figure 27: Comparison of the orbital dimensions for many of the low-mass X-ray binaries. Note that Her X-1 and 4U1626-67 are pulsars, A0620-00 is a black hole candidate, and MXB 1659-29 is one of two eclipsing bursters.[81]

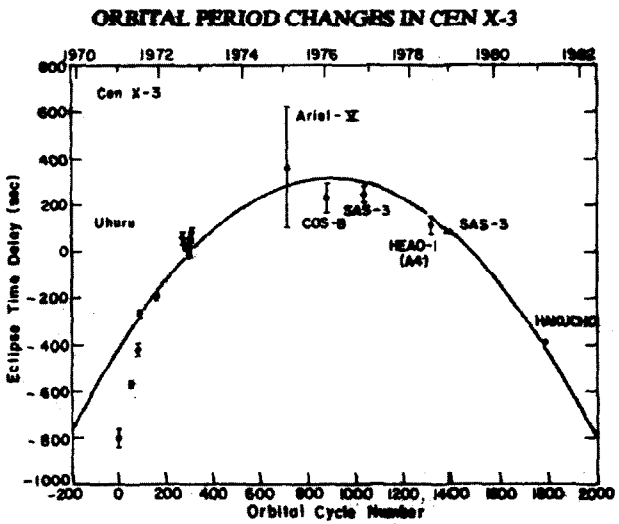

Figure 28: Decrease in the orbital period of the X-ray binary pulsar Cen X-3 as shown by the quadratic change in the arrival time of its eclipses.[84]

due to the loss of matter from the companion star in a stellar wind of 6×10^{-6} $M_\odot$ yr^{-1}. Tidal coupling between the neutron star and its companion can also produce the observed decay. In this case, the companion star is rotating asynchronously with the orbit, and the resulting tidal distortion will exert a torque which can decrease the orbital angular momentum.

By similar reasoning, orbital decay in low-mass X-ray binaries should occur at a fractional rate of $< 10^{-10}$ yr^{-1}. However, in the one eclipsing low-mass X-ray binary for which data span many years (EXO 0748-676), the observed changes in eclipse timing suggest a rate which is $\sim$ 700 times greater, and rather than decreasing, the orbital period is seen to increase! The sign and magnitude of the orbital period derivative indicates that the neutron star may be spinning down, and transferring its lost angular momentum to the binary system (see Figure 29).

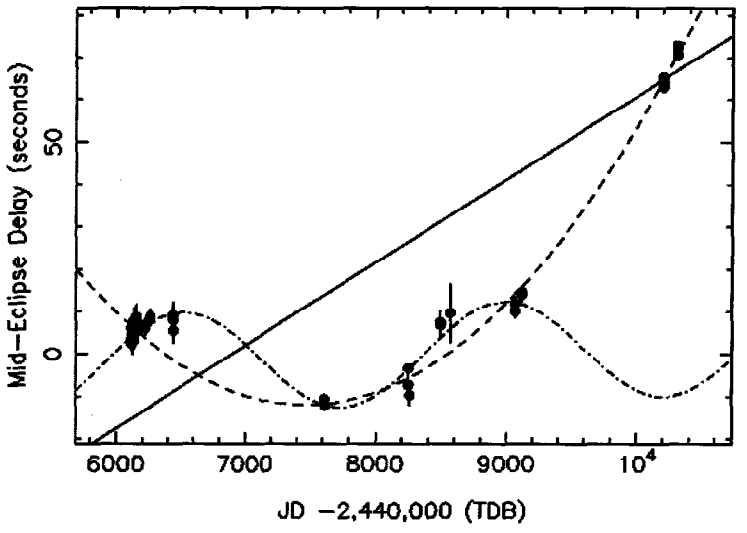

Figure 29: Change in the orbital period of the eclipsing low-mass X-ray binary EXO 0748-676 as shown by the changes in the arrival time of its eclipses. The sinusoid dot-dashed model is for a triple system. This, and the constant orbital period model (straight line) are ruled out by the long term observations. However, even the best fit, constant orbital period derivative model (dashed line) does not formally fit the data.[85]

4.5 Mass Determination in X-ray Binaries

Techniques used to determine the mass of the compact object in an X-ray binary system differ for the X-ray pulsars (six of which are in eclipsing systems) and black hole candidates. In the following sections, I will describe the methods used in each case.

4.5.1 Neutron Star Masses

For X-ray pulsars in binary systems, the derived orbital elements from Doppler shift analysis can be combined with Kepler's Third Law to derive the mass function for the compact object. The mass function is defined as:

$$f(M) = \frac{M_x^3 \sin^3 i}{M_{tot}^2} \tag{13}$$

where M_x is the mass of the compact object, i is the inclination angle to the orbital plane from our line-of-sight, and M_{tot} is the total mass in the binary system. Detailed spectroscopic studies of the companion star are then used to determine its mass by identifying its spectral type. (This process has significant uncertainties, however, in that the relationship between mass and spectral type is derived from studies of non-interacting binaries.) And for those (six) systems which show X-ray eclipses, the assumed mass-radius relationship for the companion star is then employed to find the inclination angle to the system. Figure 30 shows a summary of the mass measurements derived in this manner for the six eclipsing systems, as well as the mass measured for the Hulse-Taylor binary radio pulsar.[83] In all cases, the mass of the neutron star is consistent with 1.4 $M_\odot$.

For the LMXB QPO sources, an equation-of-state independent relation has been derived[74] that yields the mass in terms of the Keplerian orbital frequency at the marginally stable orbit, r_{ms}. Matter at r_{ms} can be related to the highest QPO frequency observed for a given source:

$$\frac{M}{M_\odot} = \frac{2198}{\nu_{max}} \tag{14}$$

Substituting the typical highest QPO frequency observed ($\sim$ 1100 Hz) yields neutron star masses of $\sim$ 2 $M_\odot$, significantly higher than those found for the neutron star pulsars. The LMXBs, however, have long been believed to be a much older population than the pulsars, and this higher mass is consistent with

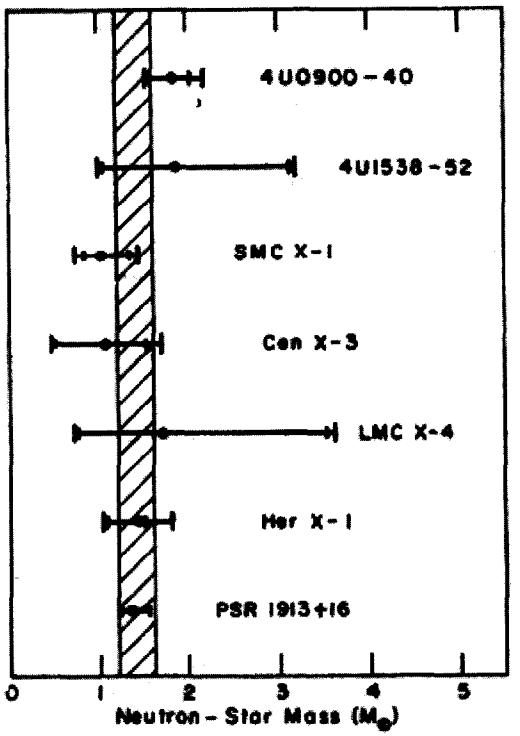

Figure 30: The masses of the six eclipsing X-ray binary pulsars and the Hulse-Taylor binary radio pulsar.[79]

accretion for $\sim 10^8$ y at $\sim 10\%$ of the Eddington limit onto the original 1.4 $M_\odot$ object created in the supernova explosion.[75,76]

4.5.2 Black Hole Candidate Masses

The determination of the orbital elements in binary systems with no detectable pulsations or no X-ray eclipses requires the use of optical data from the companion star. Radial velocity curves are obtained, with amplitude $K \sin i$ km s^{-1}, and orbital period P_{orb} (see Figure 31). These data measure the effect of the unseen compact object on its companion star, and can be related through Kepler's laws to the mass function (see Equation 13), establishing a lower limit on the mass of the unseen, X-ray emitting companion:

$$f(M) = \frac{P_{orb}\, K^3}{2\pi G} < M_x. \tag{15}$$

The lower limit to the compact object's mass M_x stems from the fact that without eclipses, it is not possible to precisely know the system's inclination angle. The angle can be estimated, however, from studies of the ellipsoidal light variations during the binary orbit. However, assuming that the companion star has a mass of zero, and that the inclination angle is 90 degrees, yields a mass function equal to the mass of the compact object. Since these are extreme values, realistic values for the mass of the companion and the inclination angle will result in a black hole mass greater than the derived mass function.

Black hole candidates are those objects for which the best estimates for the compact object's mass (after taking into account the mass of the optical companion and the inclination angle to the system) are greater than 3 $M_\odot$, the Rhoades-Ruffini upper limit to the mass of a neutron star.[86] Other common observational characteristics shared by some of the black hole candidates include two-component energy spectra, in which one component is very soft, and highly variable, transient X-ray outbursts. Roche-lobe schematics for some typical black hole candidate binaries are given in Figure 32 and Figure 33. The best black hole candidates are those in which the mass function itself is greater than $3M_\odot$. For example, in V404 Cygni[87] the mass function is 6.08 ± 0.06 $M_\odot$, and the most likely mass is $12M_\odot$.

It should be noted however, that the Rhoades-Ruffini neutron star mass limit of 3 $M_\odot$, although independent of assumptions about the specific form of the neutron star equation of state, does make certain assumptions that can be questioned. For

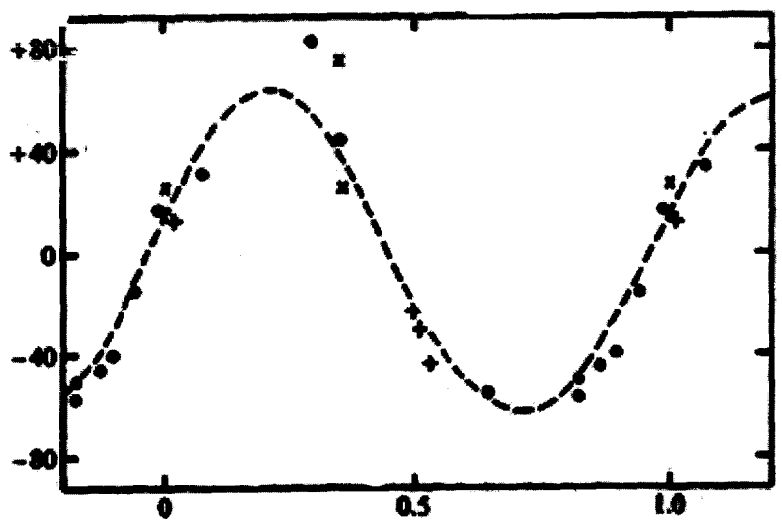

Figure 31: Optical radial velocity curve for the companion to the black hole candidate Cygnus X-1. Radial velocities are measured in km s^{-1}, and are shown as a function of phase in the 5.6 d binary orbit.[88]

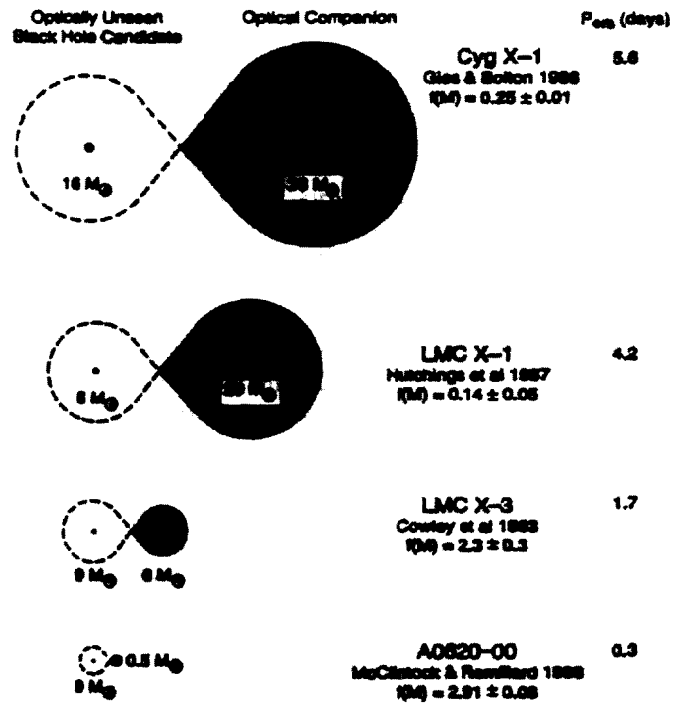

Figure 32: Roche lobe schematics for five black hole candidates.[89]

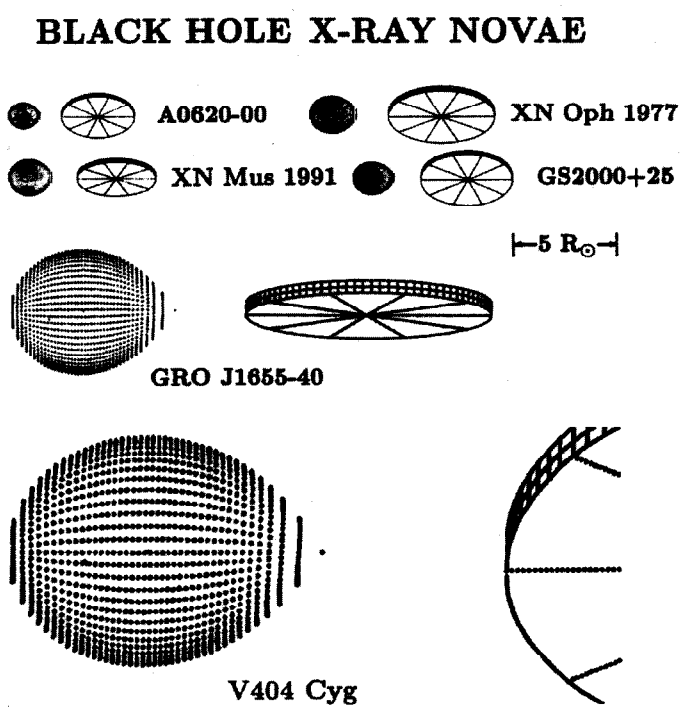

Figure 33: Roche lobe schematics for X-ray nova black hole candidates, indicating the approximate inclination angle to the line of sight to each binary system, and the size of the accretion disk around the compact object.[90] A0620-00 appears in both this figure and in Figure 32.

example, Rhoades and Ruffini assume that General Relativity provides the correct description of gravity in the strong field regime, and that gravity provides the stabilizing force which overcomes repulsive pressures in the star's core. If instead hadronic forces in the core can stabilize the star, it may be possible to increase the mass of a neutron star far above this limit.[91,92]

4.5.3 Microquasar Masses

There are two galactic black hole candidate binaries which differ markedly from those discussed in the previous section. Known as the microquasars, GRS1915+105 and GRO J1655-40 exhibit superluminal radio jets (as do extragalactic quasars), and transient, highly variable X-ray emission.[93] Because the masses of these two objects are only $\sim 10\ M_\odot$ rather than $\sim 10^6\ M_\odot$, the radii of their accretion disks and radio lobes are also about one million times smaller. The temperature of the radiation from the inner accretion disk is correspondingly higher, with the bulk of the observable emission in the X-ray bandpass. And of course, unlike their galaxy-gobbling extragalactic counterparts, the microquasars are being fueled by accreting matter from a binary companion star. This comparison is illustrated in Figure 34.

Observations of the microquasar sources with the Rossi X-ray Timing Explorer have shown QPO from both sources.[56,57] Optical observations[94] and careful analysis of ellipsoidal light variations from the eclipsed companion to GRO J1755-40 have resulted in a mass determination for the compact object of $7.02 \pm 0.22\ M_\odot$. This agrees well with the interpretation of the 300 Hz QPO from this object as resulting from matter circulating at the marginally stable orbit, r_{ms}. Applying the same argument to the 67 Hz QPO seen from GRS 1915+105 yields a mass estimate[56] of $\sim 33\ M_\odot$.

An alternative origin for the 67 Hz QPO from GRS1915+105 has been advanced by Nowak and his collaborators.[95] They interpret the QPO as diskoseismic eigenfrequencies of the microquasar's accretion disk, and derive a black hole mass ranging from 11 to 33 $M_\odot$, for systems containing Schwarzschild to maximally prograde Kerr black holes, respectively.

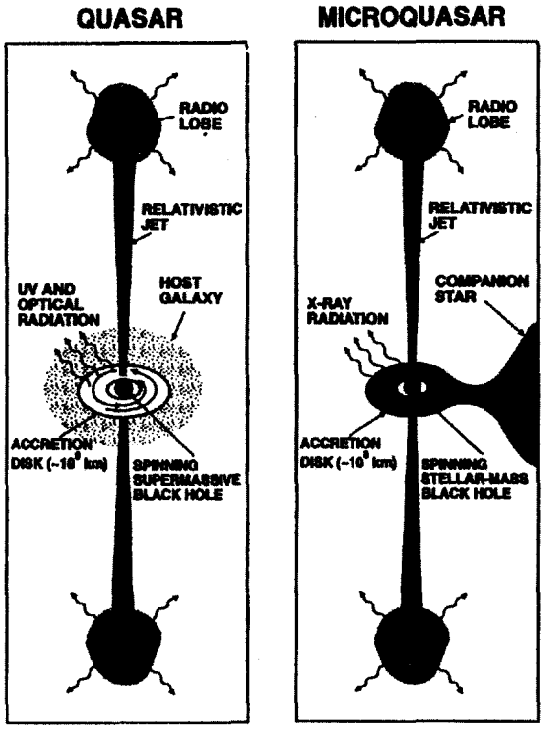

Figure 34: A comparison between extragalactic quasars and microquasar X-ray binaries.[96]

4.6 Neutron Star Equations of State

In order to use X-ray observations to learn about the neutron star equation of state, it is necessary to measure both the mass and the radius of the star for a given object.[74] Although observations of X-ray bursts have greatly constrained the mass-radius relation[31] for many of the low-mass X-ray binaries, many uncertainties remain. The energy spectra from X-ray bursts may not be perfect blackbodies; models of neutron star atmospheres have shown[97] that the color temperature T_c is greater than the effective temperature T_e by a factor of ~ 1.5. However, recent observations of the "twin-peaks" QPO, combined with X-ray burst observations, may have given us a new observational handle on the problem.[75,76]

As an example, Kaaret, Ford and Chen[75] show that the mass derived from the highest frequency QPO is typically $\sim 2M_\odot$. For the well studied X-ray burster 4U1636-53, they derive a mass of $2.02 \pm 0.12M_\odot$, where the uncertainty takes into account both the observational uncertainty in the QPO measurement, as well as additional theoretical uncertainties in the location of the emitting region responsible for the QPO, and in the moment of inertia, which depends on the equation of state. Interpreting a 4.1 ± 0.1 keV absorption feature in the spectrum of an X-ray burst from this same object as redshifted absorption from Fe XXV ions in matter accreted onto the neutron star surface, one can use Equation 10, with a mass of $2.0M_\odot$ to determine the radius. The value for the radius, found in this manner, is 9.6 ± 0.6 km. QPO have been seen in the bursts from this source, at a frequency of 581 Hz, which may be twice the neutron star spin frequency.[98] These parameters are best suited to a soft or moderately soft equation of state for a rapidly rotating neutron star, such as EOS-A or -AU, as calculated by Cook, Shapiro and Teukolsky.[99]

5 Relativistic Effects

In this final section, I review very recent, sometimes controversial evidence and ideas regarding the direct observation of relativistic effects in systems containing neutron stars and black holes.

5.1 Evidence For Event Horizons In Black Holes

Narayan and his colleagues[100,101,102] have suggested that accreting black hole binaries, when in quiescence (*i.e.*, not during a transient X-ray outburst) will have very different X-ray spectra than quiescent neutron star transients. Their advection dominated accretion flow (ADAF) models give good results for fits of the energy spectra over a wide bandpass, from optical through X-ray wavelengths. In these models, the presence of the event horizon in a black hole binary results in much lower accretion efficiency, as the advected material simply disappears over the horizon, without radiating much of the thermal energy carried in the infalling plasma. (The accretion efficiency, η, in these systems is estimated at 0.05%.) For the neutron star systems in which the infalling material shocks at the surface (or the magnetosphere) $\eta \approx 10\%$.

An additional prediction of the ADAF models is that black hole transients should have a wider dynamic range of minimum to maximum luminosities, since their quiescent states should be $\sim$ 500 times less luminous. Although hard to prove due to limited observations of non-emitting X-ray transients, there is some evidence that appears to support this prediction.[101]

5.2 Evidence For Black Hole Spin

Zhang, Cui and Chen[103] have interpreted the often seen soft-component in X-ray energy spectra from black hole candidate objects as blackbody emission from the inner accretion disk at the marginally stable orbit, r_{ms}. They have used this idea to calculate blackbody spectra for black holes with different rotation rates. Distinct spectral differences are then found in the three different spin classes: maximally prograde Kerr, Schwarzschild (slowly or non-spinning) and maximally retrograde Kerr. The accretion efficiencies η differ for these three classes of objects from 30% to 6% to 3%, as r_{ms} changes from 1 to 6 to 9 times (GM/c^2), respectively.

In this scenario, the microquasar sources contain maximally prograde Kerr black holes. The extremely high accretion efficiency ($\eta = 30\%$) coupled with the small r_{ms} raises the temperature of the inner part of the accretion disk, producing a relatively hard spectral component, in agreement with the observations.

The traditional galactic black hole candidates in binaries with a pronounced soft-component, are identified with slowly or non-rotating (Schwarzschild) black holes. And the black hole candidates which seem similar to these sources, but are lacking the spectrally-soft component are suggested to be maximally retrograde Kerr black holes. In this case, the inefficient accretion ($\eta = 3\%$) coupled with the relatively large r_{ms} combine to lower the temperature of the soft component until it falls below the standard X-ray bandpass, and is undetectable by present instruments.

5.3 Lense-Thirring Effect

Stella and Vietri[104] were the first to suggest that QPO observed in the range 20 - 40 Hz from neutron star binaries could result from the Lense-Thirring effect. If the plane of the accretion disk of material orbiting the neutron star is tilted with respect to that defined by the binary system (which is assumed aligned with the spin axis of the neutron star), then the orbiting material must precess in a prograde direction as its inertial frame is dragged along with the rotating object. The frequency of this precession in the weak field approximation is given by:

$$\nu_{LT} = \frac{8\pi^2 I \nu_K^2 \nu_s}{Mc^2} = 13.2\ I_{45}\ \mathrm{M}_\odot{}^{-1}\ \nu_{K3}^2\ \nu_{s2.5}\ \mathrm{Hz} \qquad (16)$$

where I_{45} is the moment of inertia of the neutron star in units of 10^{45} g cm^2, ν_{K3} is the Kepler frequency of the orbiting material in kHz, and $\nu_{s2.5}$ is the spin frequency of the neutron star in units of 300 Hz. Note that this interpretation assumes that the kHz QPO observed in these systems result from material orbiting at r_{ms}, and that the difference frequency from the twin kHz QPO peaks yields the neutron star spin period, ν_s. Some of the evidence in support of this conjecture is given by the quadratic dependence of ν_{LT} on ν_K. This quadratic dependence is observed in changes in the corresponding QPO frequencies from the X-ray burster MXB 1728-334.

Extending Stella and Vietri's suggestion to include black holes, Cui, Zhang and Chen[105] applied the Lense-Thirring formalism to the QPO seen in the two microquasar sources as well as several other candidate systems. For the black hole candidates, the weak field approximation used by Stella and Vietri was not appropriate, so Cui et al. modified the equations to apply to strong field systems. Assuming a mass for the candidate object and interpreting the observed QPO as the Lense-Thirring precession frequencies yielded spin rates which were found to be consistent with those in their earlier work.[103] In particular, the microquasar GRO J1655-40, which has a well-determined[94] black hole mass of $\sim 7\ \mathrm{M}_\odot$, is found to be

rotating at 95% of maximum, while the more typical black hole candidates, such as Cyg X-1 are only rotating at $\sim$ 50% of maximum. Further analysis, however, of GRO J1655-40 has complicated the picture as three other QPO frequencies have been found[57] in some observations of the source. It is therefore not clear which QPO frequency, if any, should be attributed to the effects of frame-dragging.

5.4 Jet Formation In Black Hole Systems

Perhaps the most dramatic results of observations using the Rossi X-ray Timing Explorer are those[106] of Eikenberry *et al.*, in which ground-based infrared data are combined with the X-ray data to show the first direct evidence for a connection between instabilities in the inner accretion disk around a black hole and the formation of jets emanating from outside its event horizon. As can be seen in Figure 35, the X-ray and infrared emissions are correlated at the beginnings of the flares, although with a $\sim$ 310 second lag at infrared wavelengths. As the emissions seen in the two bandpasses decouple, the X-ray luminosity begins to oscillate wildly (with a quasi-period of about 10 seconds), until it finally cuts off. The infrared emission persists and decays slowly, following the disappearance of the X-rays. The cycle then repeats about every 30 minutes.

Eikenberry and his colleagues interpret these striking results in the following manner: the initial linkage between the X-ray and infrared flares indicates that the emissions in both bandpasses are triggered by the same event. The rapidly oscillating intense X-ray luminosity is associated with activity in the inner disk. Some of the disk material is then ejected to form the longer-lasting non-thermal infrared[107] (and radio[108]) emission. These flares are similar to, but not as large as the previously observed[93] superluminal events from the same object. The subsequent disappearance of the X-ray emission may indicate that the material in the inner disk has left the system: either by falling over the black hole's event horizon or in the form of the jet material.

5.5 Gravity Wave Generation From Rotating Neutron Stars

The unexpected strength of a gravitational radiation driven instability in hot young rapidly rotating neutron stars has recently been shown[109,110] to quickly ($\sim$ 1 year) reduce the initially rapid rotation rate of the star to $\sim$ 100 Hz. The instability occurs in the $l = 2$ $r-$mode, and the resulting radiation couples to

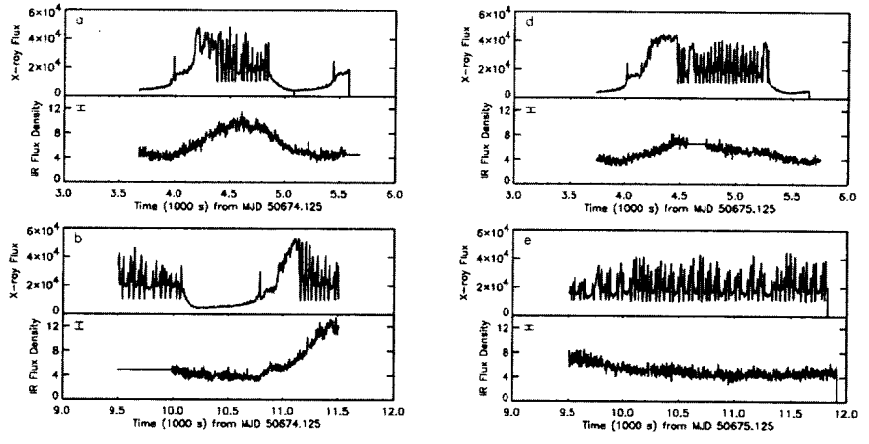

Figure 35: Coordinated infrared and X-ray observations of GRS 1915+105, a microquasar.[106]

this mode through current, rather than mass multipoles. Detectable gravitational waves may result from this process, which carries away most of the angular momentum of newly formed neutron stars.

Another mechanism for reducing the neutron star's spin rate by the emission of potentially observable gravitational radiation has been suggested by Bildsten.[111] If the thermal distribution of the neutron star's interior has a large scale asymmetry which is not aligned with its spin axis, a time varying quadrupole moment can be produced, of sufficient strength to spin down accreting neutron stars to the observed periods near 300 Hz. Unlike the previously discussed r-mode instability, this thermally driven mechanism will only affect accreting neutron stars, as the outer crust must be heated by the repeated electron captures which occur in the accreted material.

6 Summary

X-ray observations of compact objects are a powerful tool for studying gravity in the strong field regime. New information about the physical properties of black

holes and neutron stars offers the hope that predictions of General Relativity in this regime will be thoroughly examined. Evidence for relativistic effects in compact X-ray binaries has been accumulating rapidly in data from NASA's Rossi X-ray Timing Explorer. Observations of rapidly rotating neutron star systems may also lead to the first direct detection of gravitational radiation.

7 Acknowledgements

Many thanks to Tim Graves, who worked very hard getting the figures into shape, and assembling my PowerPoint presentations. Assistance from Jonathan Wong in converting one of the computer movies and in running the SLAC display projector is also greatly appreciated. This paper has greatly benefited from careful readings by J. Garrett Jernigan, whose comments were very helpful.

8 A Short Tutorial on the Names of X-ray Sources

As in ground-based astronomy, the names of objects in the X-ray sky are a combination of history and convenience, and may seem mysterious to the uninitiated. In the 1960s, X-ray observations were done with rocket-borne instrumentation. The positional information returned from these types of experiments was often crude (a few degrees), resulting in names for the newly discovered sources such as Sco X-1 (the first X-ray source found in the constellation Scorpius) or Cen X-3 (the third source found in the constellation Centaurus). As positional information improved, and particularly for sources located near the center of our Galaxy, and along the Galactic plane, the names evolved to approximate the positions in galactic coordinates. For example, GX 339-4 is located near a galactic longitude of 339 degrees and latitude -4 degrees.

With the launch of the Uhuru satellite in 1970, came the first all-sky survey. The subsequent improvement in source positions (to much less than 0.1 square degrees in most cases) required a different naming system. The Fourth Uhuru catalog[112] lists $\sim$ 350 X-ray sources, with names like 4U1617-15 (Sco X-1), where the 4U represents the catalog name, and the source location is now given in right ascension and declination (similar to the Earth's longitude and latitude). Sco X-1 is located near 16 hours, 17 minutes of right ascension, and near -15 degrees in declination. The numbers are truncated, not rounded, and usually don't change in common usage, even when the positions improve. Sometimes, additional digits will be added (*e.g.*, MXB1728-334, which is near a declination of -33.4 degrees). Many other satellites have discovered sources that are not in the 4U catalog, and lend their initials as prefixes to positional numbers. For example, the English Ariel satellite (A), European EXOSAT satellite (EXO), the MIT X-ray burst (MXB) and persistent (2S) sources discovered with SAS-3, the Vela satellites (V), or the Italian BeppoSAX satellite (SAX).

If not otherwise indicated, positionally derived names are given in 1950 coordinates (the actual positions of the sources change continually as the earth's coordinate system precesses with respect to its astronomical equivalent). As we approach the year 2000, it has become more convenient to name sources according to the positions that they will have in that Julian year. This has led to names such as GRO J1655-40 or GRO J1744-28 (Compton Gamma-ray Observatory discovered sources given in J2000 coordinates.) But when referring to radio pulsars, it is still common to use Besselian 1950 coordinates, which are designated with the letter B (*e.g.*, PSR B1259-63). Some of the other sources referred to in this paper were discovered by the Russian-French satellite Granat (GRS 1915+105), are named after their optical counterparts (V404 Cyg) or are soft gamma repeaters (SGR 1806-20).

9 Glossary

Accretion: The process of gravity-driven mass transfer. In X-ray binaries, the accretion flow leaves the companion star and ends up at the compact object.

Apastron: In an eccentric binary orbit, the distance of greatest separation between the stars.

Be-star: A main-sequence companion star often associated with neutron star pulsars in X-ray binaries. Be-stars are of spectral type B (surface temperatures $\sim$10,000 K), and also show emission lines. They have a typical mass of 5 - 10 $M_\odot$, and are rotating very rapidly. The rotation rate is near break-up, which often causes the outer layers of the star to be spontaneously ejected (even for isolated Be-stars), triggering a transient X-ray flare in those binary systems with orbiting neutron stars.

Burster or *X-ray Burst Source*: A neutron star which emits occasional very intense flashes of X-ray emission. Bursts last for 10-20 seconds, and recur on timescales of hours to days. They are interpreted as thermonuclear flashes occurring in the surface layers of the neutron star. Thermonuclear bursts are often referred to as *Type I*, to distinguish them from the very rapid *Type II* bursts which are believed to result from instabilities in the accretion flow.

Eddington limit: The critical luminosity where the outward force from radiation pressure balances the inward gravitational force on the accreting matter, and hence stops the accretion flow. The Eddington luminosity is given by:

$$L_{Edd} = \frac{4\pi G M m_p c}{\sigma_T} = 1.3 \times 10^{38} \left(\frac{\mathrm{M}}{\mathrm{M}_\odot}\right) \text{ ergs s}^{-1}. \quad (17)$$

In the above equation, M is the mass of the accreting object, m_p is the mass of a proton (assuming hydrogen plasma accretion), and σ_T is the Thomson cross-section for electron scattering.

Equation of State: The equation $P = P(\rho)$, which determines the relationship between the mass and radius for compact objects. Equations of state (EOS) vary from *soft* to *stiff*. In a soft EOS, the average system energy is attractive when nuclear density ($\rho_{nuc} = 2.8 \times 10^{14}$ g cm^{-3}) is reached. For stiff EOS, energy from repulsive interactions dominates at densities greater than nuclear. This extra pressure against gravitational collapse produces neutron stars with higher maximum masses, larger radii for a given mass, thicker crusts and lower central densities.

Lense-Thirring effect: A prediction of General Relativity, first worked out by physicists W. Lense and H. Thirring in 1918. They realized that a torque-free gyroscope will precess relative to an inertial frame at infinity. For X-ray binaries, this translates into the observational effect that particles in accretion disks which are inclined with respect to the spin axis of the compact object may precess as they orbit around it. Another way to say this is that rotating bodies have the ability to drag their inertial frame (*i.e.*, space and time) around with them as they rotate. Hence this effect is often known as *frame-dragging*.

$\mathrm{M}_\odot$: One solar mass, $\sim 2 \times 10^{33}$ grams.

Magnetar: A neutron star with an extremely intense magnetic field, $B \approx 10^{14} - 10^{15}$ Gauss. Starquakes causing magnetic reconnection in the surface layers of magnetars have recently been suggested as the cause of the bursts seen from the *Soft Gamma-ray Repeaters*.

Microquasar: An accreting black hole binary which shows superluminally expanding radio jets. The jets are similar to, but much smaller than those seen in extragalactic quasars.

Periastron: In an eccentric binary orbit, the distance of closest approach between the stars.

Prograde: A system in which the accreting material has the same angular momentum vector direction as does the spin vector for the compact object. In prograde systems, the accreting object should spin up as it accretes material.

Pulsar: A rotating neutron star that emits strictly periodic pulsations. These can be found both isolated and in binary systems.

Pulsar Wind: A relativistic positron/electron plasma which is emitted from isolated, rotating neutron stars. The wind is powered by the loss of rotational kinetic energy as the pulsar's spin slows.

Quality or *Q-factor*: This is defined in a power spectrum as $Q = \frac{\nu}{\Delta\nu}$. It is used to characterize the sharpness of the observed spectral peaks.

Retrograde: A system in which the accreting material has the opposite angular momentum vector direction to the spin vector for the compact object. In retrograde systems, the accreting object should spin down as it accretes material.

Quasi-periodic Oscillations: Regular pulses that occur at slightly changing frequencies. QPO are seen from both neutron stars and black holes in X-ray binaries.

Roche lobe: The gravitational equipotential surface in a binary system. *Roche lobe overflow* is an accretion mechanism where the slowly evolving low-mass companion star's outer layers expand outside of the Roche lobe. Matter can then be transferred through the inner Lagrangian (L_1) point to the vicinity of the compact object. Typical accretion rates with this mechanism are around 10^{-10} $\mathrm{M}_\odot$ yr^{-1}.

Stellar Wind Capture: The mass transfer mechanism typically found in high-mass X-ray binary systems. The rapidly evolving high-mass companion star sheds copious material (usually hydrogen plasma) in an outgoing wind, some of which can be captured by the compact object. Typical mass loss rates are around 10^{-6} $\mathrm{M}_\odot$ yr^{-1}; of this, perhaps 1% is captured by the compact object.

X-ray binary: A white dwarf, neutron star, or black hole with a companion star that is usually on the *main sequence*, *i.e.*, burning nuclear fuel in its core. The conventional way to refer to these systems is to classify them according to the

mass of their companion stars. A *high mass X-ray binary* has a companion star that is more massive than 5 $M_\odot$, while a *low-mass X-ray binary* has a companion star less massive than 2 $M_\odot$.

X-ray transient or *X-ray nova*: A binary system in which transient, intense X-ray emission is visible for a duration of ~months out of ~years. Transient emission can be seen from both black hole and neutron star X-ray binaries.

References

[1] R. Giacconi et al., Phys. Rev. Letters **9**, 439 (1962).

[2] A. Hewish et al., Nature **217**, 709 (1968).

[3] T. Gold, Nature **218**, 731 (1968).

[4] A. G. Lyne and F. Graham-Smith, *Pulsar Astronomy*, (Cambridge University Press, Cambridge, 1990), **16**.

[5] J. K. Daugherty and A. K. Harding, ApJ **252**, 337 (1982).

[6] K. S. Cheng, C. Ho and M. A. Ruderman, ApJ **300**, 522 (1986).

[7] R. W. Romani and I.-A. Yadigaroglu, ApJ **438**, 314 (1995). See also http://astrophys.stanford.edu/home/ion/pulsar/frames.html

[8] http://cossc.gsfc.nasa.gov

[9] D. Bhattacharya in *X-ray Binaries*, edited by W. H. G. Lewin, J. van Paradijs and E. P. J. van den Heuvel, (Cambridge University Press, Cambridge, 1995), **26**, pp. 233-251.

[10] S. R. Kulkarni and J. J. Hester, Nature **335**, 801 (1988).

[11] S. R. Kulkarni et al., Nature **359**, 300 (1992).

[12] L. Cominsky, M. Roberts and S. Johnston, ApJ **427**, 978 (1994).

[13] S. Johnston et al., ApJ **387**, L37 (1992).

[14] M. Tavani, J. Arons and V. M. Kaspi, ApJ **433**, L37 (1994).

[15] V. M. Kaspi et al., ApJ **453**, 424 (1995).

[16] M. Hirayama et al., submitted to ApJ (1998).

[17] C. Thompson and R. Duncan, MNRAS **275**, 255, (1995).

[18] C. Thompson and R. Duncan, ApJ **473**, 322 (1996).

[19] J. E. Grove et al., ApJ **447**, L113 (1995).

[20] C. Kouveliotou et al., IAU Circ. No. 6944, see also http://www.magnetars.com and http://ssl.berkeley.edu/ipn3/sgr1627-41

[21] C. Kouveliotou et al., Nature **393**, 235 (1998).

[22] *X-ray Binaries*, edited by W. H. G. Lewin, J. van Paradijs and E. P. J. van den Heuvel, (Cambridge University Press, Cambridge, 1995), **26**.

[23] J. Frank, A. King and D. Raine, *Accretion Power in Astrophysics*, (Cambridge University Press, Cambridge, 1992), **21**.

[24] J. Blondin's web site: http://www.physics.ncsu.edu/people/faculty.html. This site has excellent movies which show his numerical simulations of various types of accretion in X-ray binaries.

[25] J. E. Grindlay et al., ApJ **205**, L127 (1976).

[26] R. D. Belian, J. P. Connor and W. D. Evans, ApJ **206**, L135 (1976).

[27] S. E. Woosley and R. E. Taam, Nature **263**, 101 (1976).

[28] P. C. Joss, Nature **270**, 310 (1977).

[29] M. Y. Fujimoto, T. Hanawa and S. Miyaji, ApJ **247**, 267 (1981).

[30] P. C. Joss, Comments on Ap. **8**, 109 (1979).

[31] N. E. White, F. Nagase and A. N. Parmar in *X-ray Binaries*, edited by W. H. G. Lewin, J. van Paradijs and E. P. J. van den Heuvel, (Cambridge University Press, Cambridge, 1995) **26**, pp. 1-57.

[32] R. Wijnands and M. van der Klis, Nature **394**, 344 (1998).

[33] N. E. White, J. H. Swank and S. S. Holt, ApJ **270**, 711 (1983).

[34] R. H. D. Corbet, A&A **141**, 91, (1984).

[35] P. C. Joss and F. K. Li, ApJ **238**, 287, (1980).

[36] L. Bildsten, in *The Many Faces of Neutron Stars*, edited by R. Buccheri, A. Alpar and J. van Paradijs, (Kluwer, Dordrecht, 1998), pp. 419-449.

[37] W. H. G. Lewin, J. van Paradijs and R. E. Taam in *X-ray Binaries*, edited by W. H. G. Lewin, J. van Paradijs and E. P. J. van den Heuvel, (Cambridge University Press, Cambridge, 1995), **26**, pp. 175 - 232.

[38] L. Cominsky and K. Wood, ApJ **283**, 765 (1984).

[39] A. N. Parmar et al., ApJ **308**, 199, (1986).

[40] J. H. Swank et al., ApJ **212**, L73 (1977).

[41] J. A. Hoffman, L. Cominsky and W. H. G. Lewin, ApJ **240**, L27 (1980).

[42] J. van Paradijs, Nature **274**, 650 (1978).

[43] T. E. Strohmayer et al., ApJ **469**, L9 (1996).

[44] W. H. G. Lewin et al., ApJ **207**, L95, (1976).

[45] J. A. Hoffman, H. L. Marshall and W. H. G. Lewin, Nature **271**, 630 (1978).

[46] C. Kouveliotou et al., Nature **379**, 799 (1996).

[47] M. H. Finger et al., Nature **381**, 291 (1996).

[48] S. Rappaport and P. Joss, ApJ **486**, 435 (1997).

[49] D. Chakrabarty and E. H. Morgan, Nature **394**, 346 (1998).

[50] J. J. M. in't Zand et al., A&A **331**, L25 (1998).

[51] W. Cui, E. H. Morgan and L. G. Titarchuk, ApJ **504**, L27 (1998).

[52] L. Cominsky, Ph. D. Thesis at the Massachusetts Institute of Technology (1981).

[53] W. H. G. Lewin, Annals New York Acad. Sci. **302**, 210 (1977).

[54] T. Takeshima et al., PASJ **43**, L43 (1991).

[55] M. van der Klis in *X-ray Binaries*, edited by W. H. G. Lewin, J. van Paradijs and E. P. J. van den Heuvel, (Cambridge University Press, Cambridge, 1995) **26**, pp. 252 - 307.

[56] E. H. Morgan, R. A. Remillard and J. Greiner, ApJ **482**, 993 (1997).

[57] R. A. Remillard et al., ApJ in press or http://xxx.lanl.gov/astro-ph/9806049 (1998).

[58] M. van der Klis et al., Nature **316**, 225 (1985).

[59] M. A. Alpar and J. Shaham, Nature **316**, 239 (1985).

[60] S. Miyamoto et al., ApJ **383**, 784 (1991).

[61] G. Hasinger and M. van der Klis, A&A **225**, 79 (1989).

[62] T. E. Strohmayer, W. Zhang and J. H. Swank, IAU Circ. No. 6320 (1996).

[63] M. van der Klis,in *The Many Faces of Neutron Stars*, edited by R. Buccheri, A. Alpar and J. van Paradijs, (Kluwer, Dordrecht, 1998), pp. 337-368.

[64] M. C. Miller, F. K. Lamb and D. Psaltis, ApJ, in press (December 1, 1998).

[65] M. van der Klis and R. A. D. Wijnands, ApJ **481**, L97 (1997).

[66] R. I. Klein et al., ApJ **469**, L119 (1996).

[67] D. Psaltis et al., ApJL **501**, L95 (1998).

[68] P. Ghosh and F. K. Lamb, ApJ **232**, 259 (1979).

[69] P. Ghosh and F. K. Lamb, ApJ **234**, 296 (1979).

[70] L. Cominsky et al., Nature **273**, 367 (1978).

[71] L. Bildsten et al., ApJS **113**, 367 (1997).

[72] R. W. Nelson et al., ApJ **488**, L117 (1997).

[73] S. L. Shapiro and S. A. Teukolsky, *Black Holes, White Dwarfs and Neutron Stars*, (John Wiley and Sons, New York, 1983) p. 382.

[74] W. Kluzniak, P. Michelson and R. V. Wagoner, ApJ **358**, 538 (1990).

[75] P. Kaaret, E. C. Ford and K. Chen, ApJ **480**, L27 (1997).

[76] W. Zhang, T. E. Strohmayer and J. H. Swank, ApJ **482**, L167 (1997).

[77] Adapted from K. R. Lang, *Astrophysical Formulae*, (Springer-Verlag, Berlin, 1986), p. 541.

[78] F. Primini, S. Rappaport, and P. C. Joss, ApJ **217**, 543 (1977).

[79] S. Rappaport and P. C. Joss in *Accretion Driven Stellar X-ray Sources*, edited by W. H. G. Lewin and E. P. van den Heuvel, (Cambridge University Press, Cambridge, 1983) p. 1 - 39.

[80] S. A. Rappaport et al., ApJ **224**, L1 (1978).

[81] P. A. Charles and F. D. Seward, *Exploring the X-ray Universe*, (Cambridge University Press, Cambridge, 1995).

[82] M. Milgrom, A&A **67**, L25 (1978).

[83] R. A. Hulse and J. H. Taylor, ApJ **195**, L51 (1975).

[84] R. Kelley et al., ApJ **268**, 790 (1983).

[85] P. Hertz, K. S. Wood and L. R. Cominsky, ApJ **486**, 1000 (1997).

[86] C. E. Rhoades and R. Ruffini, Phys. Rev. Lett. **32**, 324 (1974).

[87] J. Casares and P. A. Charles, MNRAS **271**, L5 (1994).

[88] B. L. Webster and P. Murdin, Nature **235**, 37 (1972).

[89] Adapted from E. D. Bloom in *Particle Physics, Astrophysics and Cosmology*, edited by J. Chan and L. de Porcel (Stanford University, Stanford, 1996) p. 159.

[90] Adapted from J. Orosz, private communication through J. E. McClintock (1998).

[91] S. Bahcall, B. W. Lynn and S. B. Selipsky, Nucl. Phys. B **325**, 606 (1989).

[92] J. C. Miller, T. Shahbaz, and L. A. Nolan, MNRAS **294**, L25 (1998).

[93] I. F. Mirabel and L. F. Rodriguez, Nature **371**, 46 (1994).

[94] J. A. Orosz and C. D. Bailyn, ApJ **477**, 876 (1997).

[95] M. A. Nowak et al., ApJ **477**, L91 (1977).

[96] I. F. Mirabel and L. F. Rodriguez, Nature **392**, 673 (1998).

[97] W. H. G. Lewin, J. van Paradijs and R. E. Taam, Sp. Sci. Rev. **62**, 223 (1993).

[98] T. E. Strohmayer et al., ApJ **498**, L135 (1998).

[99] G. B. Cook, S. L. Shapiro and S. A. Teukolsky, ApJ **424**, 823 (1994).

[100] R. Narayan and I. Yi, ApJ **428**, L13 (1994).

[101] R. Narayan, M. R. Garcia and J. E. McClintock, ApJ **478**, L79 (1997).

[102] R. Narayan, D. Barret and J. E. McClintock, ApJ **482**, 448 (1997).

[103] S. N. Zhang, W. Cui and W. Chen, ApJ **482**, L155 (1997).

[104] L. Stella and M. Vietri, ApJ **492**, L59 (1998).

[105] W. Cui, S. N. Zhang and W. Chen, ApJ **492**, L53 (1998).

[106] S. S. Eikenberry et al., ApJ **494**, L61 (1998).

[107] R. P. Fender et al., MNRAS **290**, L65 (1997).

[108] L. F. Rodriguez and I. F. Mirabel, ApJ **474**, L123 (1997).

[109] L. Lindblom, B. J. Owen and S. M. Morsink, Phys. Rev. Lett. **80**, 4843 (1998).

[110] B. J. Owen et al., Phys. Rev. D **58**, in press (Oct. 15, 1998).

[111] L. Bildsten, ApJ **501**, L89 (1998).

[112] W. Forman et al., ApJS **38**, 357 (1978).